Research Square

Preprints are preliminary reports that have not undergone peer review.
They should not be considered conclusive, used to inform clinical practice,
or referenced by the media as validated information.

Reassignment of virulence function within the WOPR transcription factor family in Aspergillus fumigatus

Scott Filler

sfiller@ucla.edu

David Geffen School of Medicine at UCLA https://orcid.org/0000-0001-7278-3700

Hong Liu

The Lundquist Institute for Biomedical Innovation

Sanjoy Paul

University of Iowa

Vigendra Arya

University of Iowa

Mark Stamnes

University of Iowa https://orcid.org/0000-0002-5869-7985

Jianfeng Lin

Lundquist Institute for Biomedical Innovation at Harbor-UCLA Medical Center

Quynh Phan

The Lundquist Institute for Biomedical Innovation

Norma Solis

Division of Infectious Diseases, Lundquist Institute for Biomedical Innovation at Harbor-UCLA Medical Center

Vincent Bruno

University of Maryland, Baltimore https://orcid.org/0000-0003-1683-2015

William Moye-Rowley

University of Iowa https://orcid.org/0000-0002-7163-1120

Article

Keywords:

Posted Date: November 26th, 2026

DOI: https://doi.org/10.21203/rs.3.rs-11722356/v1

License: This work is licensed under a Creative Commons Attribution 4.0 International License.
Read Full License

Additional Declarations: There is **NO** Competing Interest.

Reassignment of virulence function within the WOPR transcription factor family in *Aspergillus fumigatus*

Hong Liu[1], Sanjoy Paul[2], Vijendra Arya[2], Mark A. Stamnes[2], Jianfeng Lin[1], Q. Trang Phan[1], Norma V. Solis[1], Vincent M. Bruno[3], W. Scott Moye-Rowley[2]*, Scott G. Filler[1,4]*

[1]Division of Infectious Diseases, Lundquist Institute for Biomedical Innovation at Harbor-UCLA Medical Center, Torrance, CA 90502 USA

[2]Department of Molecular Physiology and Biophysics, Carver College of Medicine, University of Iowa, Iowa City, IA, 52242, USA

[3]Department of Microbiology and Immunology and Institute for Genome Sciences, University of Maryland School of Medicine, Baltimore, MD 21201 USA

[4]Department of Medicine, David Geffen School of Medicine at UCLA, Los Angeles, CA 90024 USA

*Correspondence: W. Scott Moye-Rowley scott-moye-rowley@uiowa.edu Scott G. Filler sfiller@ucla.edu

Most fungi contain two members of the WOPR family of fungal-specific transcription factors. One member is similar to *Candida albicans* Wor1 and typically required for virulence. The other is similar to *Schizosaccharomyces pombe* Pac2 but dispensable for virulence. We found that WOPR transcription factors function differently in *A. fumigatus*. Deletion of OsaA, the *A. fumigatus* ortholog of Wor1, had no effect on virulence, whereas deletion of WrpA, the Pac2 ortholog, profoundly attenuated virulence by reducing damage to pulmonary epithelial cells and increasing susceptibility to phagocyte killing. Using RNA-seq, chromatin-immunoprecipitation-sequencing and mutant analysis, we determined that WrpA forms a network with the Ndt80 and NscR transcription factors. This network controls the expression of *ArrB*, an arrestin gene, and determines the capacity of *A. fumigatus* to cause a lethal infection and withstand macrophage killing in the lungs of immunosuppressed mice. Thus, the WrpA-Ndt80-NscR circuit is a key regulator of *A. fumigatus* virulence.

The fungus *Aspergillus fumigatus* causes progressive, invasive pulmonary disease that can disseminate hematogenously. Risk factors for invasive aspergillosis include chemotherapy, corticosteroids, advanced HIV infection, anti-TNF therapy, and solid organ or stem cell transplantation [1]. Up to 28% of patients with severe COVID-19 infections who required mechanical ventilation had possible or probable invasive aspergillosis [2]. Despite the introduction of new antifungal agents for the treatment of invasive aspergillosis, the mortality of this infection exceeds 30% and is substantially higher when the infecting strain is resistant to the azole antifungal agents [3,4]. The morbidity, mortality, and financial costs of invasive aspergillosis are expected to increase as the number of patients at risk rises due to more aggressive chemotherapy and transplantation protocols, coupled with the increasing prevalence of azole-resistant isolates. It is thus critical to develop novel therapeutic strategies to prevent and treat invasive aspergillosis. To do so, it is essential to understand the mechanisms that underlie the pathogenesis of this disease.

The WOPR (Wor1, Pac2, Ryp1) family of transcription factors is fungal-specific [5]. Most fungi possess two different WOPR family members, one that is similar to *Candida albicans* Wor1 and one that is similar to *Schizosaccharomyces pombe* Pac2 (Figure 1A). The Wor1-related members of this family control virulence in multiple fungal species, including *C. albicans* (Wor1)*, Histoplasma capsulatum* (Ryp1), *Coccidioides posadasii* (Ryp1), *Cryptococcus neoformans* (Rcv1), and *Fusarium oxysporum* (Sge1) [5-13]. Although Wor1 orthologs regulate virulence in all of these fungi, each ortholog does so through distinct mechanisms. In *C. albicans,* Wor1 is the master regulator of white-opaque switching, which controls mating and virulence in specific anatomic niches [14]. By contrast, *Histoplasma* Ryp1 controls virulence by regulating the hyphae to yeast transition [8], while *Coccidioides* Ryp1 regulates virulence by controlling the formation of spherules [12]. Both Ryp1 orthologs control virulence-related traits by regulating the levels of other transcription factors [15,16]. In phytopathogens, Wor1 orthologs direct the production of a unique set of secondary metabolites and phytotoxins that differs with each

organism [9-11,17,18]. However, the downstream transcription factors that are regulated by these Wor1 orthologs have not yet been defined.

Here, we identified two WOPR family members in *A. fumigatus,* OsaA (AFUA_6g04490) and WrpA (Wor1, Ryp1/Reg1, Pac2; AFUA_3g09640). We investigated the roles of these transcription factors in *A. fumigatus* virulence. Unlike the situation in most fungi, OsaA, the Wor1 ortholog in *A. fumigatus,* is dispensable for virulence, whereas WrpA, the Pac2 ortholog, is essential for maximal virulence. Note that the basidiomycete *Cryptococcus* requires both the Wor1-like Rcv1 and Pac2-like Liv3 for maximal virulence [13,19,20]. Our data indicate that in *A. fumigatus,* the two branches of the WOPR family have not simply swapped roles*;* the requirement for virulence has been lost from the Wor1 branch and gained in the Pac2 branch. We discovered that WrpA acts with the Ndt80 and NscR transcription factors in a previously unrecognized network. This network has multiple targets, one of which is ArrB, an arrestin-type adaptor protein that enables *A. fumigatus* to withstand macrophage killing and cause maximal lethality in immunosuppressed mice.

Results

The transcriptional regulator WrpA governs virulence and susceptibility to phagocyte killing

To investigate the roles of *A. fumigatus* WrpA and OsaA in host cell interactions and virulence, we constructed Δ*wrpA* and Δ*osaA* mutants in the *A. fumigatus* Af293 strain background and tested their virulence during invasive aspergillosis in corticosteroid-immunosuppressed mice [21-24]. Mice infected with the Δ*wrpA* mutant had almost no mortality and markedly lower lung fungal burden relative to mice infected with the wild-type parent strain (Figures 1B and C). Complementing the Δ*wrpA* mutant with an intact copy of *wrpA* restored its virulence to wild-type levels, thus verifying the central role of *wrpA* in governing virulence. A Δ*wrpA* mutant constructed in *A. fumigatus* strain CEA10 was also highly attenuated in virulence (Figure S1A).

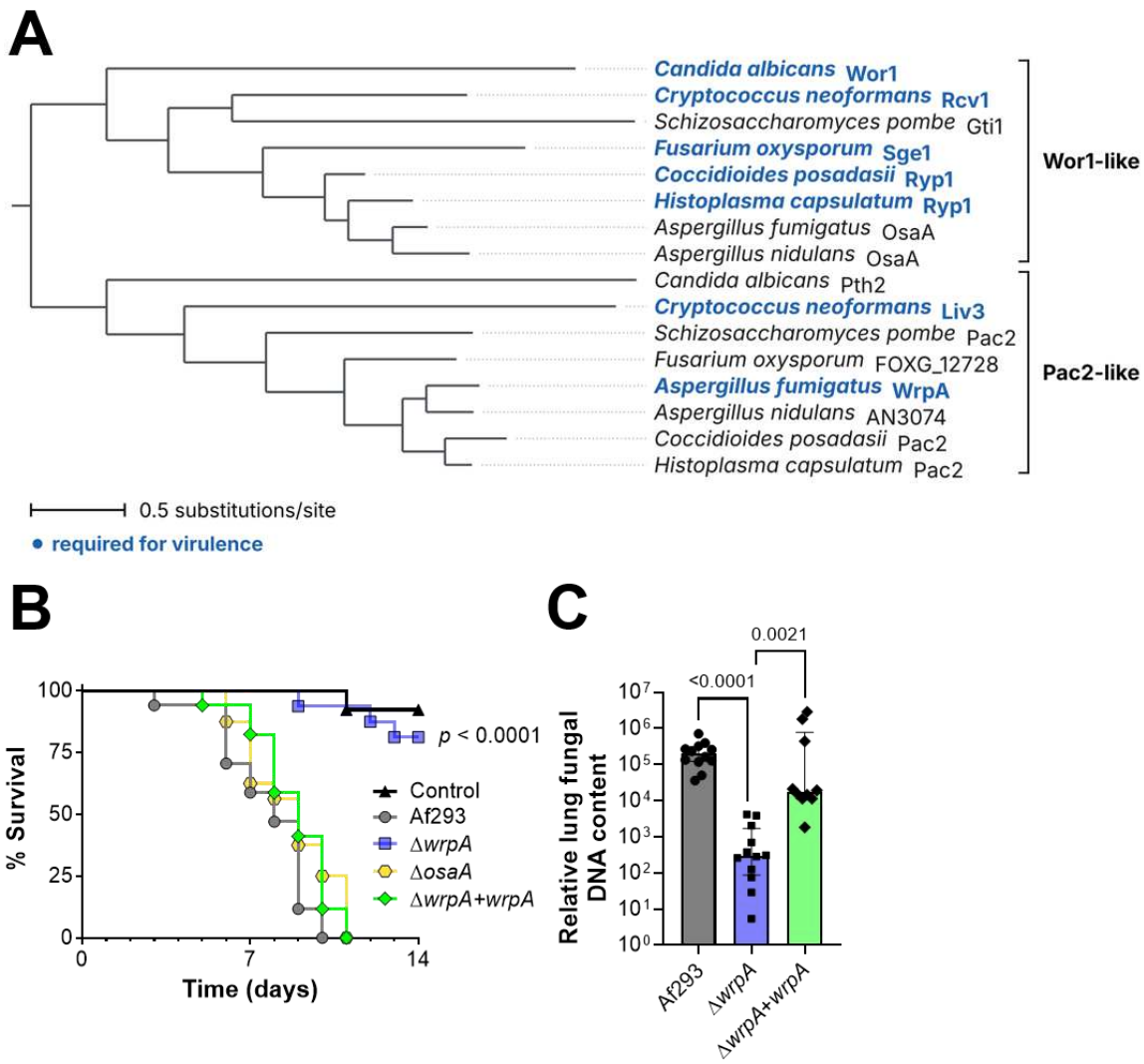

Figure 1 WrpA is a Pac2-like transcription factor that is required for maximal virulence.

(A) Maximum-likelihood phylogeny of WOPR-family proteins from selected fungi. Numbers at nodes are SH-aLRT support / ultrafast bootstrap percentages from 1,000 replicates each. The tree is rooted between the two clades. Brackets indicate the Wor1-like and Pac2-like clades. Proteins in blue are required for virulence in their respective species. Scale bar, 0.5 substitutions per site.

(B) Survival of mice immunosuppressed with cortisone acetate and then inoculated with the indicated strains of *A. fumigatus*. Results are the combined data from 2 experiments (n= 16 mice per strain). Significance determined by the log-rank test.

(C) Relative lung fungal DNA content of immunosuppressed mice after 5 days of infection. Results are median ± interquartile range of 12 mice per strain in a single experiment. Significance determined by the Kruskal-Wallis test with Dunn's multiple comparisons test.

In contrast, mice infected with the Δ*osaA* mutant died as rapidly as mice infected with the wild-type strain (Figure 1B). These results indicate that WrpA, but not OsaA, is a major regulator of pathogenicity in *A. fumigatus*.

To investigate potential causes of the virulence defect of the Δ*wrpA* mutant, we analyzed its growth in vitro. The Δ*wrpA* mutant had modestly reduced conidiation (Figure 2A) and slightly slower growth than the wild-type strain on Sabouraud agar (Figure 2B). The Δ*wrpA* mutant also had modestly increased susceptibility to voriconazole and caspofungin.

The capacity of various *A. fumigatus* mutants to damage pulmonary epithelial cells in vitro is generally predictive of their virulence in mice [21,25-29]. The Δ*wrpA* mutant caused significantly reduced damage to the A549 type II-like alveolar epithelial cell line as compared to the wild-type strain (Figure 2C). This damage defect was rescued by reintegration of an intact copy of *wrpA* into the Δ*wrpA* mutant strain. Similar results were obtained with the Δ*wrpA* mutant constructed in the CEA10 strain background (Figure S1B).

Next, we used the fluorescent Aspergillus reporter (FLARE) technique [30] to assess the interactions of wild-type and Δ*wrpA* mutant conidia with phagocytes during infection in the mouse lung. In this approach, the conidia were engineered to express DsRed and then labeled with AlexaFluor 633. Mice were inoculated with these conidia via intratracheal injection. After 18 h, the animals were sacrificed and their lungs were harvested and digested to produce a suspension of single cells, which were analyzed by flow cytometry (Figure S2). Conidia that were viable displayed fluorescence in both the DsRed and Alexafluor 633 channels whereas killed conidia lost their DsRed fluorescence and were detectable only in the Alexafluor 633 channel.

We found that infection with the Δ*wrpA* mutant did not significantly alter the accumulation of macrophages or neutrophils in the lungs relative to infection with the wild-type parent strain Af293 (Figures S3A and B). However, there was a slight reduction in the accumulation of dendritic cells in the mice infected with the Δ*wrpA* mutant (Figure S3C). This mutant was phagocytosed similarly to the parent Af293 strain by macrophages and neutrophils but had reduced phagocytosis by dendritic cells (Figures S3D-F). Of note, Δ*wrpA* conidia had

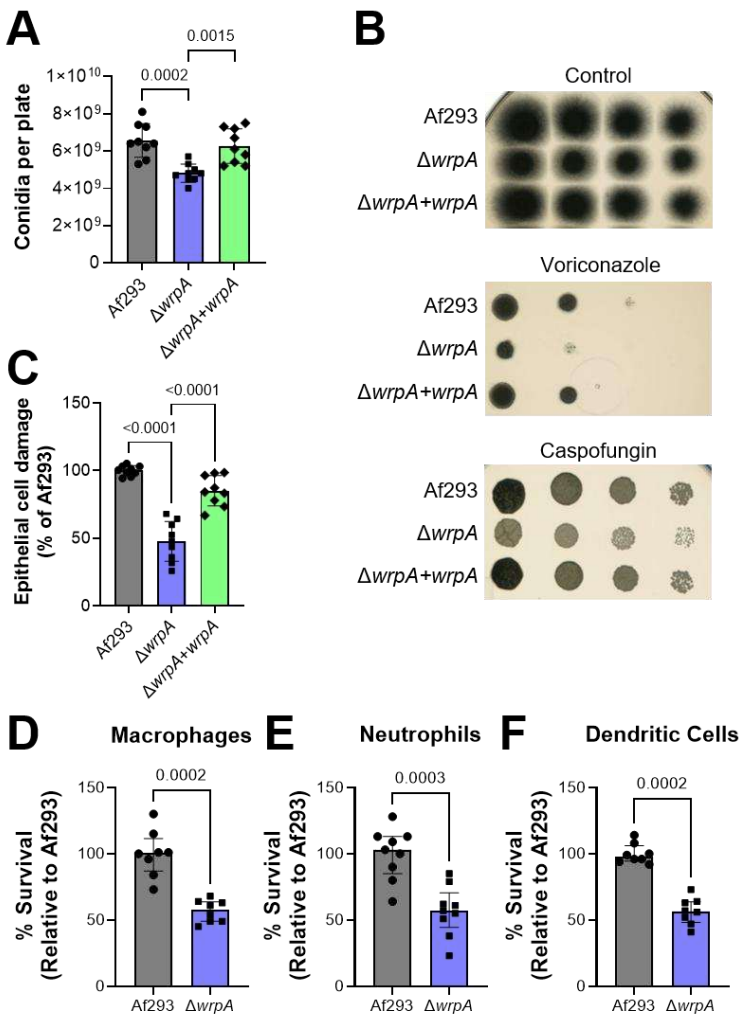

Figure 2 WrpA governs conidiation, antifungal susceptibility, epithelial cell damage and resistance to phagocyte killing.

(A) Conidia production by the indicated *A. fumigatus* strains. Results are mean ± SD of 3 experiments, each performed in triplicate. Differences were analyzed by one-way ANOVA with Šídák's multiple comparisons test.

(B) Growth on Sabouraud dextrose agar (top) and susceptibility to voriconazole (middle) and caspofungin (bottom). Plates were imaged after growth at 37°C for 48 h.

(C) Damage to A549 epithelial cells by the indicated strains after 18 h of infection. Results are mean ± SD of 3 experiments, each performed in triplicate. Differences were analyzed by one-way ANOVA with Šídák's multiple comparisons test.

(D-F) Survival of conidia of the indicated strains after phagocytosis by macrophages (D), neutrophils (E) and dendritic cells (F) in the lungs of immunosuppressed mice after 18 h of infection. Results are median ± interquartile range of 8 mice per strain in a single experiment. Significance determined by the Mann-Whitney test.

significantly reduced survival in all three types of phagocytes (Figure 2D-F), indicating that virulence defect of the Δ*wrpA* mutant is due at least in part to increased susceptibility to phagocyte killing.

WrpA controls the expression of multiple transcription factor genes

To identify WrpA target genes, we performed RNA-seq analysis of Af293 and the Δ*wrpA* mutant grown in *Aspergillus* minimal medium (AMM) with low zinc and low iron at pH 6.5, a condition that induces a transcriptional response that is similar to that induced by growth in the mouse lung [26]. We also analyzed the transcriptomes of these two strains during growth in Dulbecco's modified Eagle medium (DMEM). The two conditions differ in growth stage as well as in medium: the AMM cultures were harvested as mature hyphae at 24 h and the DMEM cultures as germlings at 6 h (after 4 h of pregermination in Sabouraud broth). We found that WrpA regulates the expression of a large percentage of genes in the *A. fumigatus* genome. A total of 1,397 and 825 genes were upregulated in the Δ*wrpA* mutant relative to the wild-type strain during growth in AMM and DMEM, respectively (Table S1 and S2). Also, 393 and 340 genes were downregulated in the Δ*wrpA* mutant in AMM and DMEM, respectively. Thus, during growth in AMM, WrpA directly or indirectly controls the expression of about 18% of the *A. fumigatus* genome.

We identified the functional classes over-represented in the WrpA regulon using the UniProt annotation of the Af293 proteome (Table 1 and Methods). Genes with significantly reduced transcript levels in the Δ*wrpA* mutant during growth in AMM were strongly enriched for components of the translational apparatus, principally ribosomal proteins (9.8-fold, FDR 1×10^{-49}), and for secondary metabolite biosynthetic genes (5.5-fold, FDR 5×10^{-6}). Deletion of *wrpA* therefore reduces the capacity for protein synthesis. Genes that were upregulated in the Δ*wrpA* mutant were enriched for transporters and permeases (1.9-fold, FDR 3×10^{-15}), oxidoreductases, enzymes acting on carbohydrates and on the cell wall, and secondary metabolite biosynthetic genes (Table 1). Deletion of *wrpA* thus altered expression of secondary metabolite biosynthetic genes in both directions.

To analyze the potential relevance of these genes during infection, we determined their expression in the lungs of immunosuppressed mice infected with *A. fumigatus* Af293, using the

data of [31]. The WrpA-dependent genes involved in translation were among the most highly expressed in the infected lung, at a median of 675 RPKM with 99% of them expressed (defined as in vivo RPKM ≥ 5), whereas the WrpA-repressed genes were largely silent in vivo, at medians of 0.1 to 4.1 RPKM with 33% to 47% expressed, against 20.4 RPKM and 71% for the genome as a whole (Table 1). As almost all of the affected secondary metabolite clusters were expressed at very low levels by the wild type strain in the infected lung, we chose not to pursue them further. WrpA therefore sustains protein synthesis under conditions that resemble the host, while many of the genes it represses in vitro have very low expression in vivo.

A possible explanation for why WrpA controls the expression of such a large number of genes is that it regulates the expression of multiple transcription factors, as has been observed with the Wor1-like WOPR family members [14,15]. Analysis of the RNA-seq datasets revealed that a common set of approximately 30 transcription factor genes was differentially expressed in the Δ*wrpA* mutant under the two growth conditions that were tested. To identify transcription factor genes that were directly regulated by WrpA, we performed chromatin-immunoprecipitation sequencing (ChIP-seq) using a strain of *A. fumigatus* that expressed WrpA with a hemagglutinin (HA) epitope tag. The strain expressing this tag caused a similar amount of damage to pulmonary epithelial cells as the wild-type strain, indicating that the epitope-tagged WrpA was functional (Figure S3G). Of the 393 genes that were downregulated in the Δ*wrpA* mutant, 71 (18.1%) were bound by WrpA (Figure 3A and Table S3). Of the 1,397 genes that were upregulated in the Δ*wrpA* mutant, 305 (21.8%) were bound by WrpA. Both overlaps exceeded chance expectation ($p = 0.030$ and $p = 2 \times 10^{-15}$, hypergeometric test).

WrpA regulates virulence in part via the Ndt80 and NscR transcription factors

Of the 1,505 genes whose promoters were occupied by WrpA, 120 encode transcription factors, 8.0% against 4.1% of the annotated genome, an enrichment of 1.95-fold ($P = 4 \times 10^{-14}$). We

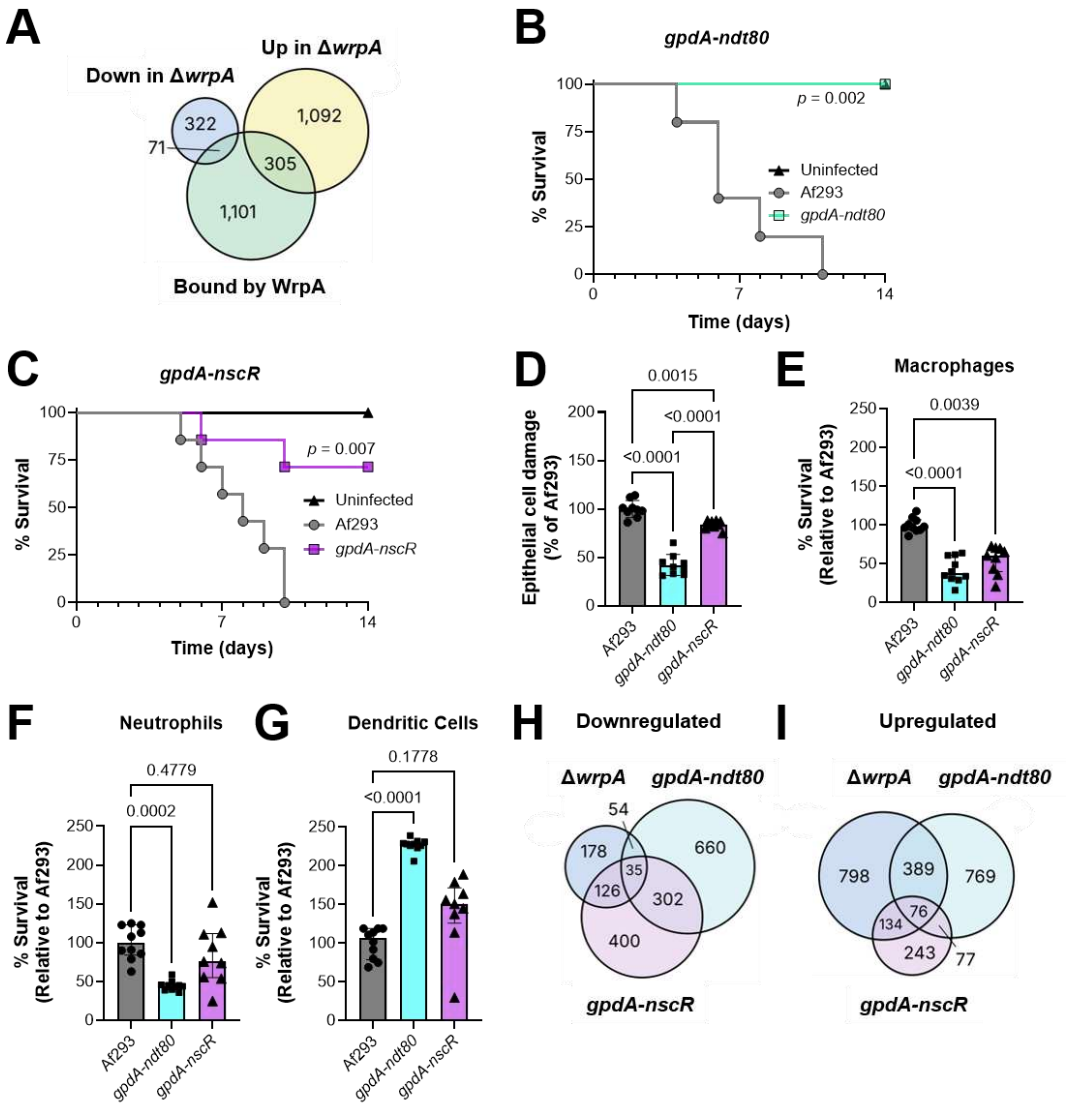

Figure 3 *ndt80* and *nscR* are targets of WrpA and govern epithelial cell damage and virulence.

(A) Venn diagram showing the relationship among genes that are differentially expressed in the Δ*wrpA* mutant and whose promoters are bound by WrpA.

(B and C) Survival of mice infected with *gpdA-ndt80* (B) and *gpdA-nscR* (C) overexpression strains. Results are from a single experiment using 5 mice per strain in (B) and 7 mice per strain in (C). Survival curves were compared using the log-rank test.

(D) Damage to A549 epithelial cells by the indicated strains after 18 h of infection. Results are mean ± SD of 3 experiments, each performed in triplicate. Significance determined by one-way ANOVA with Šídák's multiple comparisons test.

(E-G) Survival of conidia of the indicated strains after phagocytosis by macrophages (E), neutrophils (F) and dendritic cells (G) in the lungs of immunosuppressed mice after 18 of infection. Results are median ± interquartile range of 8 mice per strain in a single experiment. Significance determined by the Mann-Whitney test with Dunn's correction for multiple comparisons.

(H and I) Relationship among genes that were downregulated (H) and upregulated (I) in the Δ*wrpA*, *gpdA-ndt80,* and *gpdA-nscR* mutants relative to the wild-type strain.

135 therefore hypothesized that WrpA acts in part by occupying transcription factor promoters and

136 focused on the 27 transcription factor genes that WrpA both binds and regulates.

We hypothesized that WrpA controls the expression of multiple transcription factors that in turn regulate the interactions of *A. fumigatus* with host cells and virulence. To test this hypothesis, we searched for transcription factor genes that were regulated by WrpA under at least one of the two *in vitro* growth conditions and that were direct targets of WrpA. From this list, we selected genes with detectable expression in the corticosteroid immunosuppressed mouse model of invasive aspergillosis. These genes were identified by RNA-seq analysis of lung samples of mice with invasive aspergillosis in which SureSelect was used for enrichment of *A. fumigatus* mRNAs [31]. Our rationale was that genes with extremely low expression *in vivo* are unlikely to regulate virulence, based on our experience with both *A. fumigatus* and *C. albicans* [26,32]. We selected six transcription factor genes that met these criteria (Table 2).

Next, we investigated which of these WrpA targeted transcription factors contributed to virulence using the following strategy. For each transcription factor gene that was down-regulated in the Δ*wrpA* mutant, we used CRISPR-Cas9 to delete that gene in the wild-type Af293 strain background. For each transcription factor gene that was upregulated in the Δ*wrpA* mutant, we overexpressed that gene in Af293 by replacing its native promoter with the strong *gpdA* promoter. We then tested the virulence of these mutants in the corticosteroid-immunosuppressed mouse model of invasive aspergillosis.

Deleting the two transcription factor genes with reduced expression in the Δ*wrpA* mutant (*fcr1* and *amyR*) did not significantly attenuate virulence (Figures S4A and B). Of the four transcription factor genes that were upregulated in the Δ*wrpA* mutant, overexpression of *ndt80* and *nscR* in Af293 resulted in significantly reduced virulence (Figures 3B and C), whereas overexpression of AFUA_1g01100 and *rosA* did not (Figures S4C and D). After the majority of the virulence studies were performed, the *ndt80* annotation was subsequently updated, revising the 5′ exon and increasing the predicted protein from 605 to 666 residues (EAL93284.1, XP_077660304.1). The original 64 N-terminal residues were replaced by 125 different ones; the remaining 541 residues, including the entire NDT80 DNA-binding domain, was identical in the

two models. We verified that overexpression of longer *ndt80* allele still inhibited virulence (Figure S4E). A second independent *gpdA-nscR* overexpression mutant also had attenuated virulence (Figure S4F). The virulence defect of the *ΔwrpA* mutant is therefore due in part to the elevated expression of *ndt80* and *nscR*.

We also analyzed whether deleting *ndt80* or *nscR* in the Δ*wrpA* mutant would rescue its defect in virulence. However, the virulence of Δ*ndt80* Δ*wrpA* and Δ*nscR* Δ*wrpA* double mutants was not significantly different from that of the Δ*wrpA* single mutant (Figure S4G and H).

As the Δ*wrpA* mutant caused reduced damage to the pulmonary epithelial cell line (Figure 2C), we assessed the capacity of the *gpdA-ndt80* and *gpdA-nscR* mutants to damage these cells. Both overexpression strains caused significantly less epithelial cell damage than the wild-type strain, with the *gpdA-ndt80* mutant having a greater defect than the *gpdA-nscR* mutant (Figure 3D). These results were verified with a second set of independently constructed *gpdA-ndt80* and *gpdA-nscR* mutants (Figure S4I). Increased expression of both *ndt80* and *nscR* in the Δ*wrpA* mutant thus contributes to its defect in damaging pulmonary epithelial cells.

To determine how overexpression of *ndt80* and *nscR* alters the interactions of *A. fumigatus* with phagocytes during pulmonary infection, we used the FLARE technique. The accumulation of macrophages and neutrophils in the lungs of mice infected with the *gpdA-ndt80* and *gpdA-nscR* overexpression mutants was similar to that of mice infected with the wild-type strain (Figure S5A and B). The phagocytosis of these mutants by macrophages and neutrophils was also similar to the wild-type strain (Figures S5C and D). However, there was increased accumulation of dendritic cells in the lungs of mice infected with the *gpdA-ndt80* mutant, and these dendritic cells had increased phagocytosis of this mutant (Figures S5E and F). Both the *gpdA-ndt80* and *gpdA-nscR* strains had significantly reduced survival in macrophages (Figure 3E). The *gpdA-ndt80* mutant also had attenuated survival in neutrophils but increased survival in dendritic cells (Figures 3F and G). These results indicate that some aspects of the Δ*wrpA* phenotype, including attenuated virulence, decreased epithelial cell damage and increased

susceptibility to phagocyte killing, are due in part to increased expression of *ndt80* and *nscR.* Also, Ndt80 and NscR function downstream of WrpA through both overlapping and distinct pathways.

WrpA, Ndt80, and NscR form a transcriptional network

Common genes controlled by WrpA, Ndt80, and NscR were identified by analyzing the transcriptomes of the *gpdA-ndt80* and *gpdA-nscR* overexpression strains using RNA-seq (Tables S4 and S5) and comparing them with that of the Δ*wrpA* mutant. Overexpression of *ndt80* and *nscR* altered the expression of a subset of WrpA-responsive genes. Of the genes that had significantly decreased expression in the Δ*wrpA* mutant, 35 were also downregulated in both the *gpdA-ndt80* and *gpdA-nscR* overexpression strains (Figure 3H). Scored against the UniProt annotation, the only class over-represented among these 35 genes is two C2H2 zinc-finger proteins, AFUA_2g02080 and AFUA_3g01100 (Figure 3I, Table 3). Of the genes that had significantly increased expression in the Δ*wrpA* mutant, 76 were also up-regulated in both the *gpdA-ndt80* and *gpdA-nscR* overexpression strains (Figure 3I). These 76 genes are enriched for the classes listed in Table 3, among them short-chain dehydrogenases, sugar transporters of the major facilitator superfamily, transporters and permeases more broadly, secondary metabolite biosynthetic genes, and family 3 glycoside hydrolases and other enzymes that degrade plant cell wall polysaccharides. Very few of these genes are expressed during in vivo infection [31]. The exception is the neosartoricin cluster, whose polyketide synthase *nscA*, prenyltransferase *nscD* and lactamase-like *nscB* are among the most highly expressed genes in vivo, at 701, 4,161 and 630 RPKM, respectively. Notably, none of genes encoding 30 secondary metabolite backbone enzymes was reduced by two-fold of more in all three strains.

To determine the genetic targets of WrpA transcriptional control, we constructed *A. fumigatus* strains that expressed epitope-tagged alleles of *ndt80* and *nscR*. Because *ndt80* and *nscR* mRNA levels were low in cells grown in vitro, the expression of the epitope tagged *ndt80*

and *nscR* alleles was driven by the *gpdA* promoter. The strains overexpressing the tagged *ndt80* and *nscR* alleles had the same reduction in epithelial cell damage as those overexpressing the untagged alleles, indicating that the tagged alleles retained function (Figures S5G and H). The strains expressing the tagged alleles of *ndt80* and *nscR* were analyzed by ChIP-seq (Tables S6 and S7).

Overall, we found that there was substantial overlap among the genes that were bound by WrpA, Ndt80, and NscR. WrpA bound the largest number of genes (1,505), of which 46% were also bound by Ndt80 and/or NscR (Figure 4A). Of the 840 genes bound by Ndt80, 77% were also bound by WrpA and/or NscR, and of the 615 genes bound by NscR, 85% were also bound by WrpA and/or Ndt80. The promoters of 364 genes were bound by all three factors, compared with 8 that would be expected if the three transcription factors bound independently. These results are consistent with the model that WrpA, Ndt80, and NscR function together to regulate target gene expression in *A. fumigatus.*

The occupancy data divide the WrpA regulon into two parts that differ in composition as well as in the factors that bind them. We refer to the 364 promoters bound by all three factors as the circuit core, and to the 807 promoters bound by WrpA alone as the WrpA-only set. Scored against the UniProt annotation, these two sets contain different kinds of gene. The circuit core is enriched for transcription factors, enzymes such as chitin synthases and the Gel family of 1,3-β-glucanosyltransferases that build and remodel the cell wall, and iron acquisition; it also contains protein kinases and C2H2 zinc-finger proteins. The WrpA-only set is enriched for transporters and permeases and iron acquisition; it also contains predicted fungal specific G-protein-coupled receptors, metalloreductases, ABC multidrug transporters, a high-affinity copper transporter and secreted α-1,3-glucanases. The circuit core is therefore weighted toward transcriptional regulation and modulation of the cell surface, and the WrpA-only set toward transport and the remodeling of extracellular glycans. The two arms also differ in how much each is expressed in the host [31]. Every enriched class in the circuit core is expressed well above the genome average

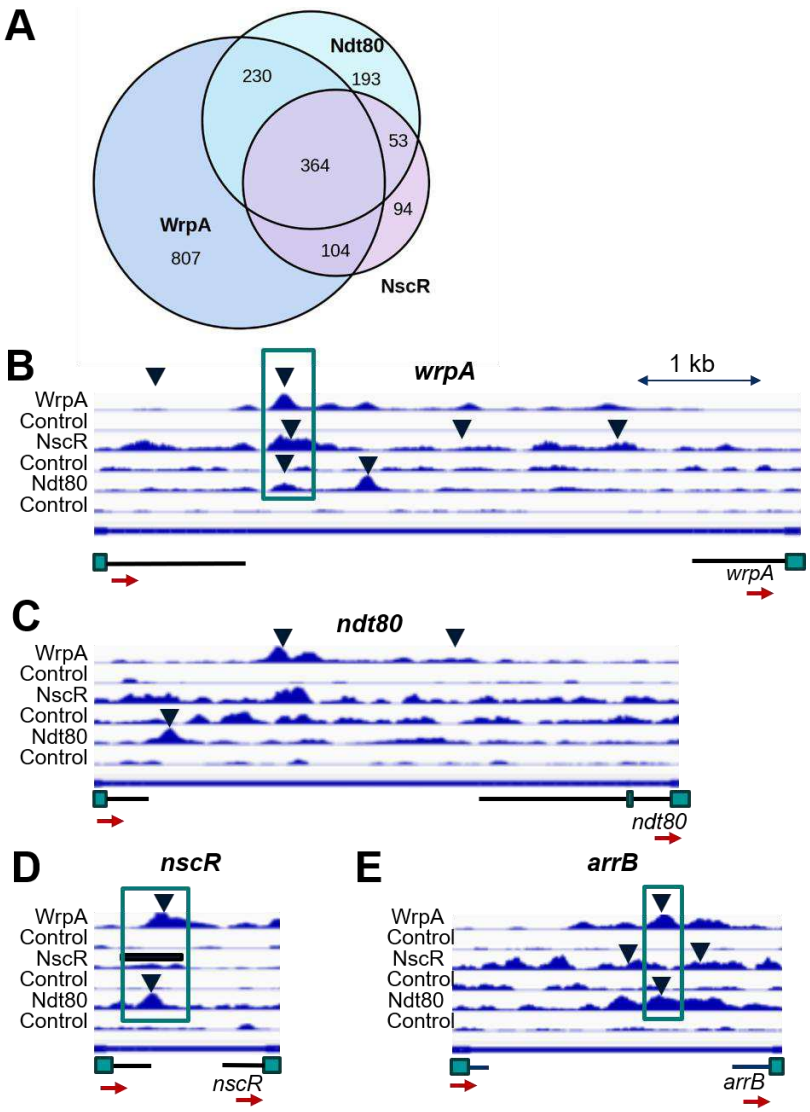

Figure 4 WrpA, Ndt80, and NscR bind to common target genes.

(A) Venn diagram showing the relationship among genes whose promoters are bound by WrpA, Ndt80, and NscR.

(B-E) ChIP-seq tracks showing the binding of WrpA, Ndt80, and NscR to the promoters of *wrpA* (B), *ndt80* (C), *nscR* (D), and *arrB* (E). Arrowheads mark called peaks (statistically enriched binding regions). Teal boxes highlight peak regions where multiple transcription factors bind. The gene models at the bottom of each set plots are shown. The green boxes indicate the open reading frames, the black lines indicate the promoter/flanking sequences, and the red arrows indicate the transcription direction.

241 in the infected lung, at medians of 60 to 206 RPKM with 70% to 100% of members expressed,

242 whereas the WrpA-only classes sit close to the genome average, at medians of 19 to 50 RPKM

243 with 67% to 88% expressed (Table 4).

We queried whether WrpA bound to any consensus sequences in the promoters of these two sets of genes. Searching the WrpA peaks for over-represented elements returned a 10-bp site, aaGCTTAAtt. Matched for peak strength, this element is enriched 21.9-fold at the positions WrpA occupies in the WrpA-only set but only 3.1-fold at circuit-core positions. It is centered on the WrpA summit, with 45% of occurrences falling within 30 bp of it against 21% expected. This observation suggests that WrpA controls the two arms of its regulon by different routes. WrpA binds to a unique site in the WrpA-only genes whereas it acts combinatorially with Ndt80 and NscR in the circuit core genes.

A further 334 promoters were bound by WrpA with only one of its partners: 230 with Ndt80 and 104 with NscR. The two classes encode different proteins. The 230 genes bound by WrpA–Ndt80 show no program of their own; their only enrichments are a weak excess of transporters (1.7-fold, FDR 0.05) and fungal specific G-protein-coupled receptors (4.2-fold, FDR 0.04), the same receptor family that were in the WrpA-only set. The 104 genes bound by WrpA–NscR are highly enriched for transcription factors, at 3.5-fold (FDR 3×10^{-4}) as compared to 2.6-fold for the circuit core and 1.6-fold for the WrpA-only set. Genes bound by WrpA–NscR are also enriched for transporters (2.3-fold, FDR 0.04), including the ABC multidrug pumps, *mdr1* and *mfsA*. There were no consensus sequences in the promoters of the genes bound by WrpA and either Ndt80 or NscR.

For select genes, we examined the predicted binding regions of the three transcription factors to determine their spatial relationship. Although WrpA, NscR, and Ndt80 bound to multiple regions along the *wrpA* promoter, one of these regions appeared to be similar for all three transcription factors (Figure 4B). Only WrpA and Ndt80 bound to the *ndt80* promoter, and the binding regions for these transcription factors did not overlap (Figure 4C). NscR bound to a broad region of the *nscR* promoter, and WrpA and Ndt80 bound to smaller regions; all three of these regions appeared to overlap (Figure 4D). All three transcription factors also bound to the promoter of *arrB*, a gene encoding an arrestin that we will discuss in detail below. In the case of

arrB, the binding regions of WrpA and Ndt80 overlapped (Figure 4E). In general, WrpA, Ndt80, and NscR have overlapping binding regions at only a subset of their target genes.

Further analysis showed that the promoters of transcription factor genes were more likely than those of other genes to be bound by all three factors, by a factor of 2.6 (10.7% against 4.1%, $P = 3 \times 10^{-8}$, Fisher exact test). This enrichment holds up when the analysis is corrected for gene expression levels. The genes bound by all three factors included 39 transcription factors, among them the developmental regulators *flbD*, *steA* and *medA*. This result supports the model that a major function of the WrpA–Ndt80–NscR circuit is to govern the expression of other transcription factors.

Combining the ChIP-seq and RNA-seq data indicated that WrpA, Ndt80, and NscR function in a circuit in which WrpA directly inhibits the expression of *ndt80* and *nscR* (Figure 5A). Ndt80 also directly inhibits the expression of *wrpA* and *nscR.* NscR indirectly inhibits the expression of *ndt80* but does not control expression of *wrpA.* Ndt80 bound 3.4 kb upstream of its own promoter. NscR also bound to its own promoter, and the NscR self-peak was the strongest in that dataset. These results suggest that both transcription factors autoregulate; additional experiments are required to verify this. Finally, the circuit contains two coupled double-negative loops, one between WrpA and Ndt80 and one between Ndt80 and NscR. In each pair, the two factors inhibit one another. This type of architecture predicts a switch-like rather than a graded behavior; the circuit is expected to sit in one state or the other and to change state only when an input is large enough to flip it. Transcriptional profiling of *A. fumigatus* recovered from the lungs of corticosteroid-immunosuppressed mice [31] indicates that *nscR* transcript is abundant, at 119 RPKM, the 88th percentile of the transcriptome, whereas *ndt80* transcript is low, at 9 RPKM, the 35th percentile and 13-fold below *nscR*. These levels are those expected if the circuit is held with *nscR* expressed and *ndt80* repressed in the infected lung, although transcript levels from a single condition cannot by themselves distinguish a discrete state from a graded setting.

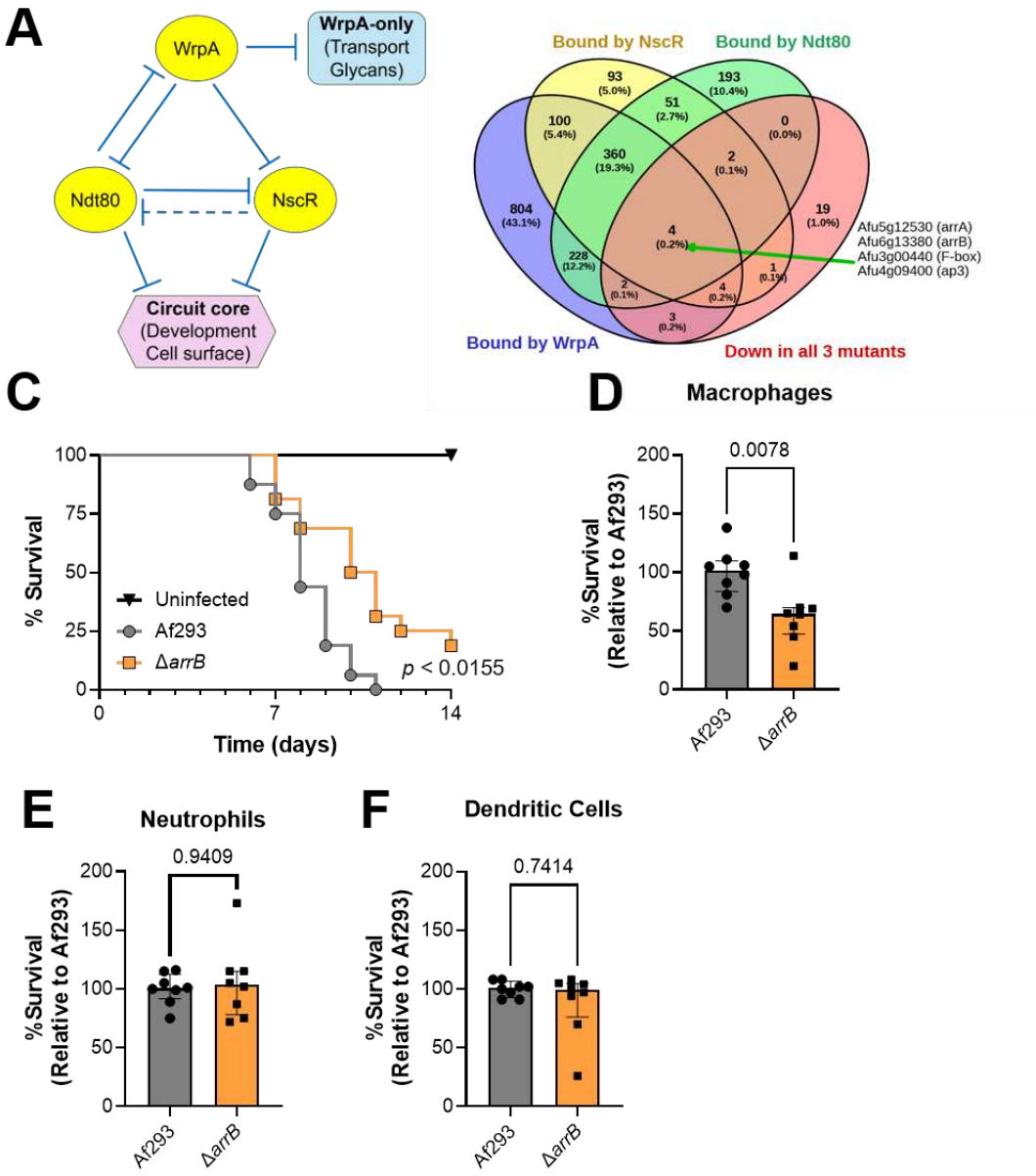

Figure 5 Two arrestins are targets of WrpA, Ndt80, and NscR.

(A) Working model of the WrpA-Ndt80-NscR regulatory circuit and its output. Dashed line indicates that NscR inhibits Ndt80 indirectly. WrpA also occupies every circuit-core promoter, but its deletion produces no net change in their expression; the core's transcriptional control comes from Ndt80 and NscR.

(B) Venn diagram showing the relationship among genes whose promoters are bound by WrpA, Ndt80, and NscR and whose mRNA levels are significantly decreased in the Δ*wrpA*, *gpdA-ndt80,* and *gpdA-nscR* mutants.

(C) Survival of mice infected with the Δ*arrB* mutant. Results are from a single experiment with 8 mice per strain. Significance determined by the log-rank test.

(D-F) Survival of conidia of the indicated strains after phagocytosis by macrophages (D), neutrophils (E) and dendritic cells (F) in the lungs of immunosuppressed mice after 18 of infection. Results are median ± interquartile range of 8 mice per strain in a single experiment. Significance determined by the Mann-Whitney test.

An arrestin is a target of the WrpA-Ndt80-NscR transcriptional circuit

We analyzed the RNA-seq and ChIP-seq data to identify genes that were either upregulated or downregulated in all three mutants and whose promoters were bound by all three transcription factors. None of the common upregulated genes met these criteria. However, 4 genes were downregulated in all 3 mutants and had promoters bound by all 3 transcription factors (Figure 5B). These genes included AFUA_3g00440, which encodes a predicted F-box protein, and AFUA_4g09400 (*ap3*), which encodes a predicted peptidase. The two other genes were AFUA_5g12530, AFUA_6g13380, which are predicted to encode arrestins, and we named them *arrA* and *arrB*, respectively.

Arrestins are scaffolding proteins that coordinate multiple cellular responses in fungi [33,34]. To analyze the function of ArrA and ArrB, we deleted the corresponding genes in strain Af293 and tested the virulence of the resulting mutants. The survival of mice infected with the Δ*arrA* mutant was similar to that of mice infected with Af293 (Figure S6A). Mice infected with the Δ*arrB* mutant survived significantly longer than those infected with Af293 (Figure 5C). This result was verified by testing a second, independent Δ*arrB* mutant (Figure S6B), demonstrating that ArrB is necessary for normal *A. fumigatus* virulence.

To determine how ArrB contributes to virulence, we tested the capacity of the Δ*arrB* mutant to damage pulmonary epithelial cells in vitro and its susceptibility to phagocyte killing in the mouse model of invasive aspergillosis. The Δ*arrB* mutant caused a similar amount of epithelial cell damage as did the wild-type strain (Figure S6C). In mice infected with the Δ*arrB* mutant, the accumulation of macrophages, neutrophils, and dendritic cells in the lungs was not significantly different from mice infected with the wild-type strain (Figures S6D-F). Also, the phagocytosis of the Δ*arrB* mutant by these leukocytes was similar to the wild-type strain (Figure S6G-I). Notably, the survival of Δ*arrB* mutant in macrophages, but not neutrophils or dendritic cells, was significantly lower than the wild-type strain (Figure 5D-F). Collectively these results

suggest that WrpA, Ndt80, and NscR all regulate the expression of *arrB*, which is required for resistance to macrophage killing and maximal lethality (Figure 5A).

ArrB associates with ubiquitin-dependent machinery and a fungal specific G protein coupled receptor

To identify proteins that associate with ArrB, we used a modified TurboID proximity labeling approach. We constructed an *A. fumigatus* strain that expressed a single chain anti-GFP nanobody [35] fused to the TurboID biotin ligase (GFPNb-tID) under control of the doxycycline-on (Dox-on) promoter. We engineered this strain to express ArrB with a functional GFP tag attached to its C-terminus. In the presence of doxycycline, GFPNb-tID was expressed and the resulting protein bound to the GFP tag on ArrB, where it biotinylated it and the surrounding proteins. We extracted the proteins from this strain and isolated those containing biotin using streptavidin beads. After extensive rinsing, the proteins were enzymatically cleaved from the beads and analyzed by MS-MS. The experiments were performed in triplicate and a strain that expressed GFPNb-tID without GFP was used as a negative control. The identified proteins were sorted by their $\log_2$ enrichment compared to the no GFP control and we only considered those with a Benjamini-Hochberg adjusted p-value of <0.05.

Of 82 proteins that reached significance, 23 were enriched with ArrB-GFP (Table S8). One of these was ArrB itself, which was the most strongly enriched protein in the dataset ($\log_2$ fold change 7.80, $q = 8.3 \times 10^{-11}$). The 22 remaining proteins had differing functions. One group of proteins comprised components of the ubiquitin-proteasome system. It included a ubiquitin-conjugating (E2) enzyme AFUA_3g13060, which was the strongest hit after the bait, the RING protein AFUA_5g05790, a proteasome activator subunit, and the E3 ligase AFUA_3g14000. These proteins may act on ArrB itself, on a substrate presented by ArrB, or both. Notably, the machinery used by classical arrestin-related trafficking adaptors was not recovered[36]. None of

the 23 proteins enriched with ArrB-GFP was a WW domain protein, Rsp5 homolog, or ESCRT subunit, even though ArrB contains a canonical PY motif (PPEY, residues 488–491) that typically mediates the interactions of α-arrestins with the WW domains of Rsp5. Because WW–PY interactions are transient, these absences do not exclude the canonical route.

Another partner, AFUA_5g02860, is of particular interest. It is a predicted fungal-specific G-protein coupled receptor of the Pth11 family, and it is the only ArrB-associated protein whose gene is itself a target of the circuit. Its promoter carries a WrpA peak, and its transcript was reduced both in the ΔwrpA mutant and in the gpdA-ndt80 overexpression strain. Its family is over-represented among the genes bound by WrpA, by a factor of 2.4 ($p = 1 \times 10^{-4}$). Because arrestins frequently bind activated membrane receptors [37], recovering a receptor-arrestin pair from an unbiased experiment suggests that ArrB may control the activity, localization, and/or signaling of this receptor. As 7 transmembrane domain-containing membrane receptors in the Pth11 family have been shown to be required for pathogenicity in plant fungal pathogens [38], regulation of this membrane protein by WrpA and ArrB may play a key role in *A. fumigatus* pathogenicity.

Several other groups of proteins were found to associate with ArrB. One group consists of two peroxisomal membrane proteins at adjacent loci that carry two of the best q values in the dataset: WscA (AFUA_2g17080), the Woronin body sorting complex protein [39], and a Pex11-family peroxin (AFUA_2g17100) of unknown function. Woronin bodies are peroxisome-derived organelles that plug septal pores after hyphal damage, which can occur during phagocyte attack [40]. Another group comprises enzymes that synthesize nutrients the phagosome withholds: a glycinamide ribonucleotide transformylase in purine biosynthesis (AFUA_2g10855), 2-isopropylmalate synthase in leucine biosynthesis (AFUA_1g15000), and GTP cyclohydrolase II of riboflavin biosynthesis (AFUA_2g01220). A third group contains membrane and lipid-handling proteins, five of the six annotated to the endoplasmic reticulum or its membrane

contact sites: a polytopic DUF914-family membrane protein with eight predicted transmembrane helices (AFUA_5g07810), the endoplasmic reticulum lumen protein-retaining receptor Erd2 (AFUA_2g02980), an SMP-domain lipid transfer protein (AFUA_3g06130), the Sec14-family phosphatidylinositol transfer protein Sfh5 (AFUA_5g03690), and a membrane-associated glutathione S-transferase of the MAPEG family (AFUA_2g08370), together with the plasma membrane stress-response phosphatase PsrA (AFUA_1g04790). These different groups of proteins likely enable *A. fumigatus* to survive and proliferate in the phagosome. Their potential dysregulation and/or mislocalization in the Δ*arrB* mutant may be the cause of its increased susceptibility to macrophage killing. Experiments to probe the role of the ArrB-interacting proteins in *A. fumigatus* virulence are underway.

Discussion

Although most fungi possess two members of the WOPR transcription factor families, the Wor1 orthologs are usually the ones required for virulence. This paradigm is true in *C. albicans*, *H. capsulatum, C. posadasii, Fusarium spp., Ustilago maydis,* and *Botrytis cinerea* [6-12,17,18]. We found that in *A. fumigatus*, this canonical division of labor is reversed: OsaA is largely dispensable for virulence, whereas WrpA has taken over as the dominant regulator. We also determined that WrpA contributes to *A. fumigatus* virulence at least in part by functioning in a transcription factor network that contains Ndt80 and NscR. Thus, in *A. fumigatus*, virulence regulation has been rewired so that WrpA takes on the role normally carried out by orthologs of Wor1.

WOPR transcription factors function differently in the basidiomycete, *C. neoformans*. Rcv1, the Wor1 ortholog, acts on virulence by controlling capsule production and cytokinesis, whereas Liv3, the Pac2 ortholog, does so by controlling quorum sensing [13,19,20]. Thus, unlike the

396 situation in ascomycetes, both WOPR transcription factors are required for maximal virulence in
397 *C. neoformans*.
398 Our phenotypic analyses indicate that WrpA controls multiple virulence-related attributes
399 of *A. fumigatus*, including conidiation, epithelial cell damage, and resistance to killing by
400 pulmonary neutrophils, macrophages, and dendritic cells. The multiplicity of factors controlled by
401 WrpA likely explains the profound virulence defect of the Δ*wrpA* mutant in the corticosteroid
402 immunosuppressed model of invasive aspergillosis.
403 It was notable that deletion of *wrpA* in the CEA10 strain background also resulted in a
404 severe virulence defect, indicating that WrpA has similar virulence-related activity in both Af293
405 and CEA10. Dabholkar et al., reported that deletion of *osaA* in strain CEA17 (derived from
406 CEA10) caused a dramatic change in phenotype, including slow growth, diminished conidiation,
407 and attenuated virulence [41]. They did not compare Δ*osaA* with Δ*wrpA* mutants. However, we
408 observed none of these changes in our Δ*osaA* mutant. While it is possible that OsaA functions
409 differently in CEA17 vs. Af293, the more likely explanation is that *osaA* was deleted using *pyrG*
410 as the selectable marker, which is known to cause aberrant results in mouse models of infection
411 [42].
412 Although WrpA shares greater homology with Pac2 than with Wor1, it functions like
413 Wor1 in that it is part of a transcriptional network. Of the six transcription factors that we found
414 were direct targets of WrpA, Ndt80 and NscR were determined to form a mutually inhibitory
415 circuit with WrpA that governs virulence. Deletion of *wrpA* and overexpression of *ndt80* and
416 *nscR* resulted in defects in similar phenotypes including decreased lethality in mice, reduced
417 pulmonary epithelial cell damage in vitro, and increased susceptibility to macrophage killing. As
418 WrpA, Ndt80, and NscR control the expression of the circuit core genes, it is therefore probable
419 that products of the circuit core genes increase epithelial cell damage and enhance resistance
420 to macrophage killing.

Not all aspects of the Δ*wrpA* phenotype were recapitulated by overexpression of *ndt80* or *nscR*. The Δ*wrpA* mutant had decreased survival in dendritic cells, whereas the *gpdA-ndt80* and *gpdA-nscR* mutants did not. A likely explanation for this difference is that the products of the WrpA-only genes, but not the core circuit genes mediate resistance to dendritic cell killing. It is known that in *C. albicans,* the Wor1 network contains at least eight transcription factors [43]. It is therefore probable that additional transcription factors function in the WrpA network and the altered expression of these other transcription factors in the Δ*wrpA* mutant may contribute to some aspects of its phenotype. It is also possible that WrpA controls the expression of some genes directly, functioning independently of other transcription factors.

The RNA-seq data indicated that WrpA sets the expression of multiple secondary metabolite genes, both positively and negatively, which is consistent with the finding that members of the WOPR transcription factor family control secondary metabolite production in filamentous fungi [9-11]. Two lines of evidence suggest that altered secondary metabolite production is not the principal cause of the attenuated virulence of the Δ*wrpA* mutant and the *ndt80* and *nscR* overexpression strains. First, no secondary metabolite backbone enzyme was reduced in all three strains, and the only biosynthetic pathway up-regulated in all three was that of neosartoricin, which inhibits T-cell proliferation but does not damage macrophages or pulmonary epithelial cells [44]. Second, the secondary metabolite genes clusters that the circuit does control are not expressed in the host. Thirty-eight genes in five named clusters, those of the fumigaclavine, pyripyropene, fumiquinazoline, fumitremorgin and endocrocin biosynthetic pathways, were repressed in both the Δ*wrpA* mutant and the *gpdA-nscR* strain and unaffected in the *gpdA-ndt80* strain. Every one of these clusters is expressed at very low levels in the wild-type strain in the infected lung [31], so their regulation by the circuit is unlikely to be consequential during infection. Taken together, these observations indicate that altered secondary metabolite production plays a limited role in the virulence controlled by this network.

The ChIP-seq data indicated that there was substantial overlap among the genes whose promoter regions were bound by WrpA, Ndt80, and NscR. Although the DNA binding sites of the three transcription factors did not consistently overlap for most genes, all three transcription factors bound to overlapping sites of the *wrpA* and *nscR* promoters, and the WrpA and Ndt80 binding sites overlapped on the *arrB* promoter. The interactions among WrpA, Ndt80, and NscR are evidently complex and vary with the target gene.

The WrpA-Ndt80-NscR circuit itself has the topology of a switch rather than of a graded regulator, because WrpA and Ndt80 inhibit one another and Ndt80 and NscR inhibit one another. During infection in the mouse lung, *nscR* is abundantly expressed (119 RPKM, 88th percentile) but *ndt80* (9.1 RPKM, 35th percentile) is not, suggesting that the NscR side of the circuit is activated in the host. This result suggests that the attenuated virulence of the *gpdA-ndt80* strain occurred because overexpression of *ndt80* forced the switch out of its infection setting.

The attenuation of the *gpdA-nscR* strain cannot be explained in the same way, because raising *nscR* should drive the switch further into its infection setting and enhance virulence. The most likely explanation is that *nscR* was expressed at supra-physiological levels when *nscR* was driven by the *gpdA* promoter. Although *nscR* was expressed at very low levels in the wild-type strain during growth in AMM, its expression increased by 1,541-fold in the *gpdA-nscR* strain, which likely caused aberrant expression of its targets. In the *gpdA-nscR* strain grown in AMM, *arrB* expression was reduced 9.8-fold. By contrast, during infection of the lung with the wild-type strain, *nscR* was abundant, but *arrB* was also highly expressed (357 RPKM, 96th percentile). Because deletion of *arrB* alone attenuated virulence and reduced survival in macrophages, the decreased expression of *arrB*, and probably the altered expression of other virulence-associated genes, is the likely cause of the attenuated virulence of the *gpdA-nscR* strain.

The common targets of all three transcription factors that showed significant transcriptional regulation were *arrA* and *arrB*, which encode arrestins. The Δ*arrB* mutant partially phenocopied the Δ*wrpA, gpdA-ndt80,* and *gpdA-nscR* mutants in that it had reduced lethality in mice and decreased survival in pulmonary macrophages. Thus, ArrB is a major target of the WrpA transcriptional circuit. Unlike the Δ*wrpA* mutant, the Δ*arrB* mutant did not have a defect in damaging pulmonary epithelial cells or reduced survival in neutrophils and dendritic cells. These differences likely explain why the virulence defect of the Δ*arrB* mutant was not as severe as the Δ*wrpA* mutant.

In fungi, arrestins function as scaffolding proteins that are important for cytokinesis, pH sensing, stress resistance, and in the case of *Cryptococcus neoformans,* virulence [33,34,45-47]. Our proximity labeling experiment indicates that ArrB associates with multiple cytoplasmic proteins. These included a RING-box subunit of cullin-RING ligases (AFUA_5g05790), a proteasome activator (AFUA_4g11290), and a large ubiquitin-conjugating enzyme (AFUA_3g13060). The simplest explanation for this combination is that these proteins act on ArrB rather than with it, and that ArrB itself is a substrate of a ubiquitin-proteasome pathway. Arrestins are themselves ubiquitinated and degraded [48], and a proximity labeling experiment performed on an arrestin will capture the machinery that modifies the bait as readily as machinery that the bait recruits [49]. This interpretation accounts for the recovery of a proteasome activator. The absence of the ESCRT and vacuolar components that cargo delivery would require is also consistent with it, although, as noted above, that absence does not by itself exclude the vacuolar route. The architecture of AFUA_3g13060 E2 enzyme is consistent with this model. The enzyme is a 1,078-residue protein whose catalytic domain lies at the extreme C terminus behind a large region with no assigned domain. This arrangement is typically found in E2 enzymes that recognize their own substrates without a separate E3 ligase [50].

As many arrestins interact with G-protein coupled receptors [36,37], it was particularly interesting that one of the proteins associated with ArrB was the predicted fungal-specific G-

protein coupled receptor, AFUA_5g02860. This protein resembles the G-protein coupled receptors seen in *Fusarium graminearum* and *Magnaporthe grisea* that are involved in virulence in these plant pathogenic fungi [38,51]. Although the *A. fumigatus* genome is predicted to encode a large number of this type of membrane protein [52], very few have been characterized. We speculate that WrpA and ArrB are important for controlling the activity of the likely membrane receptor, AFUA_5g02860. Because of the increased susceptibility of the Δ*arrB* mutant to pulmonary macrophage killing, we speculate that ArrB and AFUA_5g02860 are required for *A. fumigatus* to withstand stress associated with being in the macrophage phagosome.

Collectively, our data show that *A. fumigatus* has repurposed a WOPR family member long considered dispensable for pathogenicity: rather than Wor1-like OsaA, it is the Pac2-like WrpA that governs virulence, acting through a circuit built with two transcription factors, Ndt80 and NscR, not previously linked to this family. This WrpA-Ndt80-NscR circuit controls the capacity of *A. fumigatus* to damage pulmonary epithelial cells and resist phagocyte killing, converging on a single downstream arrestin, ArrB, that is required for maximal virulence. These findings define a previously unrecognized virulence circuit in *A. fumigatus* and provide a framework for defining its remaining components.

Materials and Methods

Ethics statement. All mouse experiments were reviewed and authorized by the Institutional Animal Care and Use Committee (IACUC) of the Lundquist Institute for Biomedical Innovation at Harbor–UCLA Medical Center. Animals were maintained in HEPA-filtered laminar airflow cages and housed according to experimental grouping, with unrestricted access to food and water. The vivarium is operated by the Lundquist Institute in accordance with the policies and guidelines of the Office of Laboratory Animal Welfare of the Public Health Service. The facility is fully accredited by the American Association for Laboratory Animal Care.

Phylogenetic analysis. To produce phylogenetic tree for the WOPR members in *C. neoformans, C. albicans, S. pombe, F. oxysporum, A. nidulans, C. posadasii,* and *H. capsulatum*, full-length sequences were aligned with MAFFT L-INS-i and the tree inferred in IQ-TREE under the Q.YEAST+F+I+G4 model selected by ModelFinder (BIC). Numbers at nodes are SH-aLRT support / ultrafast bootstrap percentages from 1,000 replicates each; the tree is rooted between the two principal clades.

Cell lines. A549 cells were purchased from the ATCC and cultured at 37°C in 5% CO_2 in F-12 K medium (ATCC, 30-2004) supplemented with 10% fetal bovine serum (FBS) (Gemini Bio-Products) and 1% streptomycin and penicillin (Irvine Scientific). The cell line had no mycoplasma contamination, as determined using MycoAlert® Mycoplasma Detection Kit (Lonza LT07-218).

Strains growth conditions. *A. fumigatus* strain Af293 was purchased from the American Type Culture Collection (ATCC). Strain AfS35 was purchased from the Fungal Genetics Stock Center. All *A. fumigatus* strains were cultured on either Sabouraud dextrose agar (Difco) or Aspergillus minimal medium at 37°C for 7–10 days before use. Conidia were collected by gently washing the agar surface with PBS supplemented with 0.1% Tween 80 (Sigma-Aldrich). The resulting suspension was passed through a 40 μm cell strainer (Corning) to remove hyphal fragments, and conidia were quantified using a hemocytometer. For experiments examining host cell interactions with germlings, the conidia were pre-incubated in Sabouraud dextrose broth (Difco) for 5.5 h at 37°C to allow germination.

Strain construction. The Δ*wrpA* and Δ*osaA* mutant strains were constructed using a split marker strategy. Briefly, about 1.5 kb of the 5'-flanking sequences of the target genes was PCR-amplified from A293 genomic DNA using paired primers F4 and F3 (All primers are listed in

549 Table S5). The resulting fragment was cloned into plasmid pNLC106 [53]. Using the plasmid as
550 template, the 5'-flanking sequence region fused to the 5’ portion of the *hph* hygromycin
551 resistance gene was amplified by PCR using primers F4 and HY-R. Next, about 1.5 kb of the 3'-
552 flanking sequence of the target gene was PCR-amplified from A293 genomic DNA using paired
553 primers F2 and F1. The 3’ sequence of *hph* was amplified by PCR from pAN7 [54] using HYG-F
554 and HYG-R. Using the mixture of the two fragments as template, the 3'-flanking sequence
555 region of target gene linked to 3' portion of *hph* was amplified by fusion PCR with primers F1
556 and YG-R. Finally, the two fragments were used to transform Af293 protoplasts. The hygromycin
557 resistant clones were screened for the deletion of target gene by colony PCR using primers
558 Screen-F and Screen-R.
559 To construct the Δ*fcr1* (AFUA_3g05760), Δ*amyR* (AFUA_4g10160), Δ*arrA*
560 (AFUA_5g12530), and Δ*arrB* (AFUA_6g13380) deletion mutants, a transient CRISPR-Cas9
561 gene deletion system was used [55,56]. The Cas9 expression cassette was amplified from plasmid
562 pFC331 (Adgene) [56], using primers Cas9-F and Cas9-R. All primers are listed in Table S5. To
563 construct the sgRNA expression cassette, two DNA fragments were amplified from plasmid
564 pFC334 (Adgene) [56] using primers sgRNA-F and sgRNA-R1, and sgRNA-R, sgRNA-PacC-F1.
565 Next, the sgRNA expression cassette was amplified by fusion PCR of the two DNA fragments,
566 using primers sgRNA-F and sgRNA-R. The hygromycin resistance (HygR) repair template was
567 amplified from plasmid pVG2.2-hph [57] using primers Hyg-F and Hyg-R, which had about 50 bp
568 of homology to the 5’ end of the protein coding sequence of the gene and the 3’ end of the
569 protein coding sequence, respectively. The HygR repair template was mixed with the Cas9
570 cassette and the two sgRNA cassettes and then used for protoplast transformation. Hygromycin
571 resistant clones were screened for deletion of specific target genes by colony PCR using
572 primers Screen-F, Screen-R. The positive clones were also confirmed for absence of integration
573 of DNA encoding Cas9 or the gRNA, using primers Cas9-ScreenF and Cas9-ScreenR, and
574 sgRNA-ScreenF, sgRNA-ScreenR. The Δ*ndt80*Δ*wrpA* and Δ*nscR*Δ*wrpA* strains were

575 constructed using a similar strategy, with pyrithiamine and phleomycin resistance markers used
576 for selection.
577 To construct the Δ*wrpA* + *wrpA* complemented strains, a 4564 bp fragment containing
578 the WrpA protein coding sequence and approximately 2 kb of 5' flanking sequence and 1 kb of
579 3' flanking sequence was PCR-amplified from Af293 or CEA10 genomic DNA using primers
580 WrpA-Com-F and WrpA-Com-R. The resulting fragment was cloned into the NotI site of plasmid
581 p402 [58], which was used to transform the Δ*wrpA* strains. To confirm the presence of the
582 complementation plasmid, the phleomycin-resistant colonies were screened by colony PCR
583 using primers WrpA-Com-F and WrpA-Com-R to detect *wrpA*. The transcript levels of WrpA in
584 the various clones were quantified by real-time RT-PCR using primers WrpA-Realtime-F and
585 WrpA-Realtime-R. The clones in which the transcript level of WrpA was most similar to that of
586 the wild-type strain was used in all experiments.
587 To construct the Ndt80 (AFUA_2g09890), NscR (AFUA_7g00130), RosA
588 (AFUA_6g07010) and AFUA_1g01100 overexpression strains, we used the CRISPR-Cas9
589 system to replace the promoter sequence of these genes with the promoter sequence of *A.*
590 *nidulans gpdA*. The sequence containing the phleomycin resistance maker followed by the
591 *ANgpdA* promoter was amplified from plasmid pGFP-phleo [22] using primers Phleo-OE-F and
592 Phleo-OE-R. The sgRNA expression cassettes were generated as described above. These
593 fragments were used to transform Af293 and target gene transcript level in the various clones
594 was quantified by real-time RT-PCR using primers Realtime-F and Realtime-R (Table S5).
595 When constructing the *ndt80* overexpression clones, the *gpdA* promoter was placed at
596 the start codon of the gene model then available (EAL93284.1, 605 aa). A subsequent model
597 (XP_077660304.1, 666 aa) revises the 5′ exon, so the two predicted proteins differ in their first
598 64 and 125 residues respectively while sharing an identical 541-residue C-terminal region that
599 contains the entire NDT80 DNA-binding domain. A second clone expressing the full-length
600 coding sequence was constructed, and overexpression of either allele attenuated virulence.

To construct the wrpA-3X HA strain, an *A. fumigatus* codon-optimized 5X GA linker fused to a 3X HA epitope tag and the AFUA_2G08370 terminator sequence was amplified from pSP106 [59] using primers wrpA-MH-3xHA-Hph-F1 and wrpA-MH-3xHA-Hph-R1. The hph selection cassette was amplified from pSP25 [60] using primers wrpA-MH-3xHA-Hph-F2 and wrpA-MH-3xHA/ko-Hph-R2. The resulting PCR products were fused by overlap-extension PCR and subsequently amplified using primers wrpA-MH-3xHA-Hph-F3 and wrpA-MH-3xHA/ko-Hph-R3. The final fusion PCR product was transformed into the *A. fumigatus* strain Af293 together with in vitro-assembled Cas9–guide RNA ribonucleoprotein (RNP) complexes and 50-bp microhomology repair templates, as described [55], using the wrpA ko/tag 3′ crRNA and hygromycin B Gold (InvivoGen) selection in AMM, pH 7.0. Targeted integration events were screened by diagnostic PCR using primers wrpA-3xHA-US-DF and Hph-US-DR, and correct C-terminal 3X HA tagging of WrpA was further confirmed by Western blot analysis using the HA.11 (16B12) mouse monoclonal anti-HA antibody (Covance).

To generate the *gpdA-ndt80*-3XFLAG strain, a donor DNA fragment containing the 3XFLAG sequence, followed by the *Aspergillus nidulans trpC* terminator and the hygromycin-resistance marker (*hph*), was amplified from the plasmid pSP131 (*atrR* 3'-GA5-3X FLAG-loxP-Hph_pUC19) using the primers FLAG-Ndt80-Donor-F and FLAG-Ndt80-Donor-R. The resulting PCR product was introduced into the *gpdA-ndt80* strain using a CRISPR-Cas9 approach. The sgRNA sequences were generated as described above using the FLAG-Ndt80-sgRNA primers (Table S5). Correct integration of the 3XFLAG tag in hygromycin-resistant transformants was confirmed by PCR using the Ndt80-FLAG-Screen-F and Ndt80-FLAG-Screen-R primers (Table S5). Expression of the Ndt80-3XFLAG fusion protein was verified by Western blotting using an anti-FLAG antibody (F3165; Sigma-Aldrich).

The *gpdA-nscR*-3X FLAG strain in the AfS35 background was constructed in two steps: first, the *gpdA-nscR* strain was generated, followed by 3X FLAG tagging at the C-terminal. In all cases, the *gpdA* promoter was obtained from *Aspergillus nidulans* but will be referred to here as

627 *gpdA* for simplicity. A microhomology repair template containing the phleomycin resistance
628 marker cassette and the *gpdA* promoter, flanked by a 40 bp sequence homologous to the *nscR*
629 promoter region, was PCR-amplified from plasmid pRFP-phleo-gpdA using primers gpdA-NscR-
630 MH-F and gpdA-NscR-MH-R. This cassette was inserted 88 bp upstream of the nscR start
631 codon by CRISPR-Cas9-mediated genome editing using a nscR 5′ crRNA. In phleomycin-
632 resistant clones, targeted integrations for upstream and downstream junctions were screened
633 by diagnostic PCR using primers gpdA-nscR-US-DF and Phleo-US-DR. To generate the *gpdA-*
634 *nscR*-3X FLAG strain, a microhomology repair template containing the hygromycin resistance
635 marker cassette preceded by a 3X FLAG sequence, flanked by 40 bp sequences homologous
636 to the *nscR* C-terminus, was PCR-amplified from plasmid pSP131 using the primers NscR-
637 pSP131-3XFlag-MH F and NscR-pSP131-3XFlag-MH R. This cassette was integrated at the C-
638 terminus of the *nscR* gene by CRISPR-Cas9-mediated genome editing using a *nscR* 3' crRNA.
639 In hygromycin-resistant transformants, targeted integrations for upstream and downstream
640 junctions were screened by diagnostic PCR using primers nscR-3XFLAG-US-DF and Hph-US-
641 DR1. Successful tagging of both proteins was confirmed by Western blotting using an anti-
642 FLAG antibody (F3165, Sigma-Aldrich).
643 The arrB-GFP allele was generated using primers arrB-MH-gfp-Ble-F and arrB-MH-gfp-
644 Ble-R to amplify an appropriate C-terminal arrB-GFP fusion allele from plasmid gfp2.5-pSK494-
645 pRFP (procured from the Fungal Genetics Stock Centre). This cassette was transformed into
646 AfS35 cells and into the fcyB-MH-Hph-Don-4xHA-GFPNb-turboID-containing AfS35 cells. The
647 latter strain was generated via integration of a cassette from plasmid pSP154 that contains the
648 doxycycline-inducible GFP nanobody-TurboID fusion gene. This cassette was integrated into
649 the fcyB gene as described earlier [35]. The plasmid pSP154 will be deposited to AddGene
650 The Af293-DsRed strain was a gift from Tobias M Hohl, Memorial Sloan Kettering
651 Cancer Center [61]. The Δ*wrpA*-DsRed strain and Δ*arrB*-DsRed strains were constructed by
652 transforming Af293 protoplasts with gpdA-DsRed-Phleo. The RFP expressing strains of Af293,

gpdA-ndt80 and *gpdA-nscR* were constructed by transforming them with RFP-FLARE (a gift from Robert Cramer, Jr., Dartmouth College).

Mouse model of invasive aspergillosis. To assess the virulence of different strains during invasive aspergillosis, we used our cortisone acetate immunosuppressed mouse model [24,62,63]. 5-week male CD1 mice (Evigo) were immunosuppressed with cortisone acetate at 400 mg/kg administered subcutaneously every other day, starting on day -4 relative to infection and finishing on day +4. To prevent bacterial infections, enrofloxacin (Baytril, Western Medical Supply) was added to the drinking water at a final concentration of 0.005% starting on day -5 relative to infection. The mice were infected by placing them in a chamber into which $1.2x10^{10}$ conidia were aerosolized. Control mice were immunosuppressed but not infected. The mice were monitored for survival twice daily and moribund mice were humanely euthanized.

To assess pulmonary fungal burden, 12 mice per group were immunosuppressed and infected using an aerosol exposure system. At 5 days post-infection, the mice were euthanized, and their lungs were harvested. RNA was isolated using the ZR Fungal/Bacterial DNA MiniPrep™ kit according to the manufacturer's instructions. Fungal DNA levels in each sample were quantified by real-time qPCR using ASF1 and ADR1 primers (Table S5). Relative fungal burden was calculated using the $2^{-\Delta\Delta CT}$ method, with mouse GAPDH-F and GAPDH-R serving as the reference controls (Table S5).

Stress assays. To test the susceptibility of the Δ*wrpA* to voriconazole and caspofungin, serial 10-fold dilutions of conidia ranging from 10^5 to 10^2 cells in a volume of 5 µl were spotted onto Sabouraud dextrose agar plates supplemented with 0.5 µM voriconazole (NDC 25021-184-82, Bella Vida Pharmacy) and 40 µg/ml caspofungin (SML0425, Millipore Sigma). Fungal growth was analyzed after incubation at 37˚C for 48 h.

679 **Conidia production.** To measure conidial yield, 10^4 conidia were spot-inoculated at the center
680 of 100-mm Petri dishes containing Sabouraud agar. After 5 days of incubation at 37 °C, conidia
681 were collected by repeatedly washing the colony surface with PBS supplemented with 0.1%
682 Tween 80. The resulting suspension was then enumerated using a hemocytometer.
683
684 **Cell damage assay.** Damage to A549 epithelial cells induced by direct interaction with *A.*
685 *fumigatus* was quantified using our previously described ^{51}Cr release assay [25]. Briefly,
686 monolayers of host cells in a 24-well tissue culture plate were incubated with 5×10^5 conidia per
687 well for 18 h in 5% CO_2 at 37°C. Following incubation, cell damage was assessed by measuring
688 the release of ^{51}Cr into the supernatant.
689
690 **FLARE assay**. The FLARE assay was performed as described [61]. Mice were
691 immunosuppressed cortisone acetated. They were inoculated by intratracheal injection of $3 \times$
692 10^7 conidia that expressed either DsRed or RFP and were labeled with AlexaFluor 633 (Thermo
693 Fisher). After 18 h of infection, the mice were sacrificed and their lungs were harvested. They
694 were disrupted with a gentleMACs tissue dissociator (Miltenyi Biotec) to yield single cells. The
695 red blood cells were removed by treatment with ACK lysis buffer (Thermo Fisher). The resulting
696 single-cell suspension was counted and $2x10^6$ cells were used for antibody staining. The
697 antibodies used were BUV395-anti-CD45 (564279, BD), FITC-anti-Ly6G (11-9668-82,
698 Invitrogen), Pe-Cy7-anti-Ly6C (560593, BD), FITC-anti-CD103- (11-1031-82, Invitrogen), Pacific
699 Blue-anti-CD11b (NC9908052, Biolegend), Ly6B.2-AF700 (NBP213077Z), CD11C-PE-Cy7
700 (558079, BD), MHCII-AF700 (56-5321-82, Invitrogen). The staining protocols were followed as
701 previously described. The neutrophils were identified as $CD45^+Ly6G^+Ly6C^{lo}CD11b^+Ly6B.2^+$,
702 macrophages as $CD45^+CD11c^+MHCII^{var}$ and dendritic cells as $CD45^+CD11c^+MHCII^{var}CD103^-$
703 $CD11b^+$. Data were acquired using a five-laser BD FACSymphony™ A5 and analyzed with
704 Flowjo Software V10. The gating strategy is diagrammed in Figure S2.

RNA-seq analysis. For RNA-seq analysis, 1.5×10^8 conidia from each strain were inoculated into modified *Aspergillus* minimal medium lacking iron and zinc [26], and cultured at 37 °C in a shaking incubator for 24 h. In another experiment. conidia were first cultured in Sabouraud broth at 5×10^5 conidia per ml in100-mm Petri dishes for 4 h and then transferred to DMEM (10569010, Gibco) and incubated for an additional 6 h at 37 °C. The resulting biomass, mature hyphae in the former case and germlings in the latter, was harvested by filtration, and total RNA was extracted using the RNeasy Plant Mini Kit (Qiagen) according to the manufacturer's protocol. Residual genomic DNA was removed by DNase treatment using the TURBO DNA-free kit (AM1907, Invitrogen).

RNA-seq libraries were constructed, and 150-bp paired-end sequencing was performed by Genohub Inc. The resulting reads were aligned to the Af293 reference genome using the short-read aligner HISAT2. On average, approximately 40 million reads were successfully mapped per sample. Differential expression was called with DESeq2 over a universe of 10,130 genes, and genes were defined as differentially expressed if they exhibited an absolute fold change ≥ 2.0 and a false discovery rate (FDR) ≤ 0.05. All strains were analyzed in biological triplicate. The AMM cultures were grown at pH 6.6 under low zinc and low iron; because this condition induces the metal-starvation regulons in every strain including the wild type, circuit effects on iron and zinc acquisition genes are superimposed on that induction. In the deletion strains the protein-coding sequence was removed while the untranslated flanking regions are retained, so reads persist at the deleted locus and each deleted gene was excluded from its own contrast. All of the raw sequencing reads from this study are available at the NCBI GEO repository as SuperSeries GSE289503.

Functional classes were assigned from the UniProt annotation of the Af293 proteome rather than from the free-text product descriptions supplied with the expression tables. Those descriptions are not a controlled vocabulary: 9,907 genes carry 6,914 distinct strings, and 48%

state an inference rather than a category, beginning "Ortholog(s) have", "Has domain(s) with predicted", or reading "protein of unknown function", so terms cannot be counted consistently across gene sets. The UniProt table assigns at least one Pfam domain to 78% of genes and a curated protein name to 84%. Enrichment was computed over Pfam domains and over functional classes defined in advance by keyword matching against curated protein names, in each case against the annotated genes present in the expression table, using a one-sided hypergeometric test with Benjamini-Hochberg correction. Classes reaching a false discovery rate below 0.05 are reported. The same vocabulary and test were applied to the genes shared by the Δ*wrpA* mutant and both overexpression strains.

To compare the two occupancy arms, log2 fold-change distributions were compared with two-sided Mann-Whitney tests and the fraction of differentially expressed genes with Fisher exact tests, in each of the seven deletion contrasts, with Benjamini-Hochberg correction across the resulting family; effect sizes are given as the common-language effect size, the probability that a randomly chosen gene from one set shifts further than a randomly chosen gene from the other. Because circuit-core genes are more highly expressed than WrpA-only genes, and the power to call differential expression rises with expression, each comparison was repeated against expression-matched controls: baseMean was divided into 20 quantile strata across all genes in the contrast, and 5,000 samples were drawn from the WrpA-only set matching the stratum distribution of the circuit core, giving an empirical one-sided P value for the observed circuit-core median and differentially expressed fraction. Expression in the infected lung is the mean RPKM across corticosteroid-immunosuppressed mice at day 4 of infection, the time point at which lung fungal burden was measured, taken from the SureSelect-enriched data set; a gene is counted as expressed at 5 RPKM or above, a threshold met by 71% of the genome, whose median expression is 20.4 RPKM by this measure [31].

Chromatin Immunoprecipitation (ChIP). ChIP was performed as described [64]. *A. fumigatus* strains expressing C-terminally tagged WrpA-3X HA, Ndt80-3X FLAG, or NscR-3X FLAG were inoculated at a density of 1×10^6 conidia/mL into 50 ml Sabouraud dextrose medium in 250 ml baffled flasks and grown for 16 h at 30°C with shaking. Mycelia were cross-linked for 15 min at 30°C with shaking (100 rpm) in cross-linking buffer (0.4 M sucrose, 10 mM Tris-HCl [pH 8.0], 1 mM EDTA) supplemented immediately before use with 1% formaldehyde and 1 mM PMSF. Cross-linking was quenched by addition of glycine to a final concentration of 100 mM, followed by incubation for an additional 10 min. Mycelia were harvested by vacuum filtration, washed with sterile ddH_2O, flash-frozen in liquid nitrogen, and stored at −80°C until further processing.

Approximately 100 mg of frozen mycelia was ground to a fine powder in liquid nitrogen and resuspended in ChIP lysis buffer (50 mM HEPES [pH 7.5], 150 mM NaCl, 1 mM EDTA, 1% Triton X-100, 0.1% sodium deoxycholate, 0.1% SDS, 1 mM PMSF, and 1× fungal protease inhibitor cocktail [Sigma-Aldrich]). Lysates were vortexed for 2 min and divided into three aliquots in AFA Fiber Pre-Slit Snap-Cap microTUBEs (Covaris). Chromatin was sheared using an E220 Focused-ultrasonicator (Covaris) equipped with an Intensifier under the following conditions: peak incident power, 175 W; duty factor, 10%; cycles per burst, 200; treatment time, 420 s; temperature, 7°C. Following sonication, aliquots from each sample were pooled and centrifuged at 10,000 × g for 5 min at 4°C. Twenty-five microliters of the clarified chromatin preparation was reserved as an input control.

For immunoprecipitation, chromatin samples were incubated overnight at 4°C on a nutator with either anti-HA mouse monoclonal antibody (clone 2-2.2.14, Invitrogen) for WrpA-3X HA ChIP or anti-FLAG mouse monoclonal antibody (clone 66008-4-Ig, Proteintech) for Ndt80-3X FLAG and NscR-3X FLAG ChIP. Samples were subsequently incubated with washed Dynabeads Protein G (Thermo Fisher Scientific) for an additional 12 h at 4°C. Washing, reverse cross-linking, and purification of immunoprecipitated DNA were performed as previously described [64]. Purified DNA was used for downstream ChIP-seq analysis in biological duplicate.

Peaks were assigned to genes as follows. Peak coordinates and the RefSeq annotation (GCF_000002655.1, ASM265v1) are not in the same frame, and the offset is piecewise constant with a single breakpoint on each of two chromosomes: 3,509 bp is subtracted on chromosome 4 beyond position 714,995 and 100 bp added on chromosome 2 beyond position 1,874,318, with no correction required on the remaining six chromosomes. This translation was verified at 796 of 797 gene starts, and without it every gene on chromosome 4 is mis-assigned. A gene was then scored as bound when any peak of that factor overlapped the window from 1,500 bp upstream to 500 bp downstream of the RefSeq gene start, strand-aware, with peaks lying in the gene body beyond +500 excluded. All annotated genes were included, protein-coding and non-coding alike, 10,073 in total. Overlap was evaluated on the whole extent of a peak rather than on its summit, so a broad peak is credited to a gene whose window its margin reaches; peak widths ranged from 225 to 9,490 bp. Peaks were de-duplicated by peak identifier and credited to every gene whose window they overlapped, so a single intergenic peak is counted for both genes of a divergent pair. This window was chosen empirically: when each gene was binned by the distance from its start to the nearest WrpA peak, enrichment for differential expression in the Δ*wrpA* mutant was greatest between 1 kb and 250 bp upstream, remained clear to 1.5 kb upstream, was absent beyond 2 kb, and gene-body peaks beyond +1 kb behaved indistinguishably from no binding. Because most Af293 gene models lack a 5′ untranslated region, the RefSeq gene start is usually the initiator codon, so the true transcription start site generally lies somewhat further upstream. On this definition WrpA bound 1,505 genes, Ndt80 840 and NscR 615. Enrichments among bound genes were tested by one-sided hypergeometric test against the genome background and, because bound genes are expressed more highly than unbound genes, confirmed against expression-matched gene sets drawn by permutation from 20 baseMean strata.

Modified TurboID. We developed a modified TurboID proximity labeling technique based on work from the Fortwendel lab [65] in which an *A. fumigatus* codon-optimized form of the TurboID biotin ligase was expressed and found to be functional in this fungus. We inserted this form of TurboID in place of the E3 ligase gene found in a doxycycline-inducible GFP nanobody construct we described earlier[35]. This arrangement allowed us to produce, in a doxycycline-dependent manner, a GFP nanobody fused to TurboID. Into this strain (designated SPF490), we inserted a C-terminal GFP tag at the C-terminus of the arrB gene to form a strain designated SPF498. We then prepared lysates from these two strains grown in the presence of doxycycline for 16 hours and purified proteins over a streptavidin column. These columns were washed extensively and then treated with trypsin. Eluted peptides were recovered and analyzed by mass spectrometry performed at the UCLA Proteomics Research Center. All samples were analyzed in triplicate and only peptides that were enriched by log2 value of 1 or greater with a Benjamini-Hochberg-corrected adjusted P-value of <0.05 were considered for further analysis.

Acknowledgements

We thank Damian Krysan for expert scientific discussion and advice. We thank Jarrod Fortwendel for providing the Aspergillus TurboID cassette and for his insightful discussions.

Author contributions

The conceptualization of the study was carried out by H.L, S.P., W.S.M. and S.G.F. Investigation was undertaken by H.L., S.P., V.A., J.L, Q.T.P., and N.V.S., while formal analysis was conducted by H.L., S. P., M.A.S. V.M.B. W.S.M., and S.G.F. Visualization was carried out by M.A.S., W.S.M., and S.G.F. Data curation was performed by M.A.S. and W.S.M. The original draft of the manuscript was prepared by H.L., S.P., W.S.M. and S.G.F., and all authors contributed to reviewing and editing the manuscript. Supervision and funding acquisition were provided by W.S.M. and S.G.F.

Funding

This work was supported in part by NIH grants R01AI162802 and R01AI143198 to SGF and WSM.

Competing Interests

The authors declare no competing interests

Data availability

All data are either in source data or have been deposited in the NCBI GEO repository as SuperSeries GSE289503

Declaration of generative AI and AI-assisted technologies in the manuscript preparation process

During the preparation of this work, the authors used Claude (Anthropic) to assist with data analysis and manuscript editing. We have reviewed and edited the output as needed and take full responsibility for the content of the published article.

References

1 Thompson, G. R., 3rd & Young, J. H. *Aspergillus* infections. *N Engl J Med* **385**, 1496-1509, doi:10.1056/NEJMra2027424 (2021).

2 Bartoletti, M. *et al*. Epidemiology of invasive pulmonary aspergillosis among intubated patients with COVID-19: s prospective Study. *Clin Infect Dis* **73**, e3606-e3614, doi:10.1093/cid/ciaa1065 (2021).

3 Baddley, J. W. *et al*. Factors associated with mortality in transplant patients with invasive aspergillosis. *Clin Infect Dis* **50**, 1559-1567, doi:10.1086/652768 (2010).

4 Resendiz-Sharpe, A. *et al*. Prevalence of voriconazole-resistant invasive aspergillosis and its impact on mortality in haematology patients. *J Antimicrob Chemother* **74**, 2759-2766, doi:10.1093/jac/dkz258 (2019).

5 Lohse, M. B., Zordan, R. E., Cain, C. W. & Johnson, A. D. Distinct class of DNA-binding domains is exemplified by a master regulator of phenotypic switching in *Candida albicans*. *Proc Natl Acad Sci U S A* **107**, 14105-14110, doi:10.1073/pnas.1005911107 (2010).

6 Pande, K., Chen, C. & Noble, S. M. Passage through the mammalian gut triggers a phenotypic switch that promotes *Candida albicans* commensalism. *Nat Genet* **45**, 1088-1091, doi:10.1038/ng.2710 (2013).

7 Xie, J. *et al*. White-opaque switching in natural MTLa/alpha isolates of Candida albicans: evolutionary implications for roles in host adaptation, pathogenesis, and sex. *PLoS Biol* **11**, e1001525, doi:10.1371/journal.pbio.1001525 (2013).

8 Nguyen, V. Q. & Sil, A. Temperature-induced switch to the pathogenic yeast form of *Histoplasma capsulatum* requires Ryp1, a conserved transcriptional regulator. *Proc Natl Acad Sci U S A* **105**, 4880-4885, doi:10.1073/pnas.0710448105 (2008).

9 Michielse, C. B. *et al*. The Botrytis cinerea Reg1 protein, a putative transcriptional regulator, is required for pathogenicity, conidiogenesis, and the production of secondary metabolites. *Mol Plant Microbe Interact* **24**, 1074-1085, doi:10.1094/MPMI-01-11-0007 (2011).

10 Jonkers, W., Dong, Y., Broz, K. & Kistler, H. C. The Wor1-like protein Fgp1 regulates pathogenicity, toxin synthesis and reproduction in the phytopathogenic fungus *Fusarium graminearum*. *PLoS Pathog* **8**, e1002724, doi:10.1371/journal.ppat.1002724 (2012).

11 Brown, D. W., Busman, M. & Proctor, R. H. *Fusarium verticillioides SGE1* is required for full virulence and regulates expression of protein effector and secondary metabolite biosynthetic genes. *Mol Plant Microbe Interact* **27**, 809-823, doi:10.1094/MPMI-09-13-0281-R (2014).

12 Mandel, M. A. *et al*. The WOPR family protein Ryp1 is a key regulator of gene expression, development, and virulence in the thermally dimorphic fungal pathogen *Coccidioides posadasii*. *PLoS Pathog* **18**, e1009832, doi:10.1371/journal.ppat.1009832 (2022).

13 Paes, H. C. *et al*. A Wor1-like transcription factor Is essential for virulence of *Cryptococcus neoformans*. *Front Cell Infect Microbiol* **8**, 369, doi:10.3389/fcimb.2018.00369 (2018).

14 Zordan, R. E., Miller, M. G., Galgoczy, D. J., Tuch, B. B. & Johnson, A. D. Interlocking transcriptional feedback loops control white-opaque switching in *Candida albicans*. *PLoS Biol* **5**, e256, doi:10.1371/journal.pbio.0050256 (2007).
15 Beyhan, S., Gutierrez, M., Voorhies, M. & Sil, A. A temperature-responsive network links cell shape and virulence traits in a primary fungal pathogen. *PLoS Biol* **11**, e1001614, doi:10.1371/journal.pbio.1001614 (2013).
16 Homer, C. M., Voorhies, M., Walcott, K., Ochoa, E. & Sil, A. Transcriptomic atlas throughout *Coccidioides* development reveals key phase-enriched transcripts of this important fungal pathogen. *PLoS Biol* **23**, e3003066, doi:10.1371/journal.pbio.3003066 (2025).
17 Michielse, C. B. *et al*. The nuclear protein Sge1 of *Fusarium oxysporum* is required for parasitic growth. *PLoS Pathog* **5**, e1000637, doi:10.1371/journal.ppat.1000637 (2009).
18 Tollot, M. *et al*. The WOPR protein Ros1 is a master regulator of sporogenesis and late effector gene expression in the maize pathogen *Ustilago maydis*. *PLoS Pathog* **12**, e1005697, doi:10.1371/journal.ppat.1005697 (2016).
19 Homer, C. M. *et al*. Intracellular action of a secreted peptide required for fungal virulence. *Cell Host Microbe* **19**, 849-864, doi:10.1016/j.chom.2016.05.001 (2016).
20 Liu, O. W. *et al*. Systematic genetic analysis of virulence in the human fungal pathogen *Cryptococcus neoformans*. *Cell* **135**, 174-188, doi:10.1016/j.cell.2008.07.046 (2008).
21 Liu, H. *et al*. Functional convergence of gliP and aspf1 in *Aspergillus fumigatus* pathogenicity. *Virulence* **9**, 1062-1073, doi:10.1080/21505594.2018.1482182 (2018).
22 Liu, H. *et al*. *Aspergillus fumigatus* CalA binds to integrin $\alpha 5\beta 1$ and mediates host cell invasion. *Nat Microbiol* **2**, 16211, doi:10.1038/nmicrobiol.2016.211 (2016).
23 Liu, H. *et al*. *Aspergillus fumigatus* AcuM regulates both iron acquisition and gluconeogenesis. *Mol Microbiol* **78**, 1038-1054, doi:10.1111/j.1365-2958.2010.07389.x (2010).
24 Chiang, L. Y., Sheppard, D. C., Gravelat, F. N., Patterson, T. F. & Filler, S. G. *Aspergillus fumigatus* stimulates leukocyte adhesion molecules and cytokine production by endothelial cells in vitro and during invasive pulmonary disease. *Infect Immun* **76**, 3429-3438, doi:10.1128/IAI.01510-07 (2008).
25 Liu, H. *et al*. The HosA histone deacetylase regulates stress resistance, host cell interactions, and virulence in *Aspergillus fumigatus*. *Microbiol Spectr* **14**, e0403625, doi:10.1128/spectrum.04036-25 (2026).
26 Liu, H. *et al*. Determining *Aspergillus fumigatus* transcription factor expression and function during invasion of the mammalian lung. *PLoS Pathog* **17**, e1009235, doi:10.1371/journal.ppat.1009235 (2021).
27 Weichert, M. *et al*. Functional coupling between the unfolded protein response and endoplasmic reticulum/golgi Ca(2+)-ATPases promotes stress Tolerance, cell wall biosynthesis, and virulence of *Aspergillus fumigatus*. *mBio* **11**, doi:10.1128/mBio.01060-20 (2020).

28 Pongpom, M. *et al.* Divergent targets of *Aspergillus fumigatus* AcuK and AcuM transcription factors during growth in vitro versus invasive disease. *Infect Immun* **83**, 923-933, doi:10.1128/IAI.02685-14 (2015).
29 Bertuzzi, M. *et al.* The pH-responsive PacC transcription factor of *Aspergillus fumigatus* governs epithelial entry and tissue invasion during pulmonary aspergillosis. *PLoS Pathog* **10**, e1004413, doi:10.1371/journal.ppat.1004413 (2014).
30 Jhingran, A., Kasahara, S. & Hohl, T. M. Flow cytometry of lung and bronchoalveolar lavage fluid cells from mice challenged with fluorescent aspergillus reporter (FLARE) conidia. *Bio Protoc* **6**, e1927, doi:10.21769/BioProtoc.1927 (2016).
31 Chung, M. *et al.* Targeted enrichment outperforms other enrichment techniques and enables more multi-species RNA-Seq analyses. *Sci Rep* **8**, 13377, doi:10.1038/s41598-018-31420-7 (2018).
32 Xu, W. *et al.* Activation and alliance of regulatory pathways in C. albicans during mammalian infection. *PLoS Biol* **13**, e1002076, doi:10.1371/journal.pbio.1002076 (2015).
33 Herranz, S. *et al.* Arrestin-related proteins mediate pH signaling in fungi. *Proc Natl Acad Sci U S A* **102**, 12141-12146, doi:10.1073/pnas.0504776102 (2005).
34 Telzrow, C. L., Nichols, C. B., Castro-Lopez, N., Wormley, F. L., Jr. & Alspaugh, J. A. A fungal arrestin protein contributes to cell cycle progression and pathogenesis. *mBio* **10**, doi:10.1128/mBio.02682-19 (2019).
35 Paul, S. & Moye-Rowley, W. S. Regulated proteolysis of green fluorescent protein fusion proteins in *Aspergillus fumigatus*. *G3 (Bethesda)* **16**, doi:10.1093/g3journal/jkaf295 (2026).
36 Jean-Charles, P. Y., Rajiv, V. & Shenoy, S. K. Ubiquitin-related roles of beta-arrestins in endocytic trafficking and signal transduction. *J Cell Physiol* **231**, 2071-2080, doi:10.1002/jcp.25317 (2016).
37 Gurevich, V. V. & Gurevich, E. V. The structural basis of the arrestin binding to GPCRs. *Mol Cell Endocrinol* **484**, 34-41, doi:10.1016/j.mce.2019.01.019 (2019).
38 DeZwaan, T. M., Carroll, A. M., Valent, B. & Sweigard, J. A. *Magnaporthe grisea* pth11p is a novel plasma membrane protein that mediates appressorium differentiation in response to inductive substrate cues. *Plant Cell* **11**, 2013-2030, doi:10.1105/tpc.11.10.2013 (1999).
39 Leonhardt, Y., Beck, J. & Ebel, F. Functional characterization of the Woronin body protein WscA of the pathogenic mold *Aspergillus fumigatus*. *Int J Med Microbiol* **306**, 165-173, doi:10.1016/j.ijmm.2016.03.008 (2016).
40 Beck, J., Echtenacher, B. & Ebel, F. Woronin bodies, their impact on stress resistance and virulence of the pathogenic mould *Aspergillus fumigatus* and their anchoring at the septal pore of filamentous Ascomycota. *Mol Microbiol* **89**, 857-871, doi:10.1111/mmi.12316 (2013).
41 Dabholkar, A. *et al.* Role of the *osaA* gene in *Aspergillus fumigatus* development, secondary netabolism and virulence. *J Fungi (Basel)* **10**, doi:10.3390/jof10020103 (2024).

42 D'Enfert, C. *et al*. Attenuated virulence of uridine-uracil auxotrophs of *Aspergillus fumigatus*. *Infect Immun* **64**, 4401-4405, doi:10.1128/iai.64.10.4401-4405.1996 (1996).
43 Noble, S. M., Gianetti, B. A. & Witchley, J. N. *Candida albicans* cell-type switching and functional plasticity in the mammalian host. *Nat Rev Microbiol* **15**, 96-108, doi:10.1038/nrmicro.2016.157 (2017).
44 Chooi, Y. H. *et al*. Genome mining of a prenylated and immunosuppressive polyketide from pathogenic fungi. *Org Lett* **15**, 780-783, doi:10.1021/ol303435y (2013).
45 du Plooy, L. M. *et al*. A fungal ubiquitin ligase and arrestin binding partner contribute to pathogenesis and survival during cellular stress. *mBio* **15**, e0098124, doi:10.1128/mbio.00981-24 (2024).
46 Zhou, L. *et al*. Arrestin-coding genes regulate endocytosis, sporulation, pathogenicity, and stress resistance in *Arthrobotrys oligospora*. *Front Cell Infect Microbiol* **12**, 754333, doi:10.3389/fcimb.2022.754333 (2022).
47 Dong, B. *et al*. Autophagy-associated alpha-arrestin signaling is required for conidiogenous cell development in *Magnaporthe oryzae*. *Sci Rep* **6**, 30963, doi:10.1038/srep30963 (2016).
48 Wedegaertner, H., Bosompra, O., Kufareva, I. & Trejo, J. Divergent regulation of alpha-arrestin ARRDC3 function by ubiquitination. *Mol Biol Cell* **34**, ar93, doi:10.1091/mbc.E23-02-0055 (2023).
49 Mukhopadhyay, U. *et al*. A ubiquitin-specific, proximity-based labeling approach for the identification of ubiquitin ligase substrates. *Sci Adv* **10**, eadp3000, doi:10.1126/sciadv.adp3000 (2024).
50 Yip, M. C. J., Sedor, S. F. & Shao, S. Mechanism of client selection by the protein quality-control factor UBE2O. *Nat Struct Mol Biol* **29**, 774-780, doi:10.1038/s41594-022-00807-6 (2022).
51 Jiang, C. *et al*. An expanded subfamily of G-protein-coupled receptor genes in *Fusarium graminearum* required for wheat infection. *Nat Microbiol* **4**, 1582-1591, doi:10.1038/s41564-019-0468-8 (2019).
52 Grice, C. M., Bertuzzi, M. & Bignell, E. M. Receptor-mediated signaling in *Aspergillus fumigatus*. *Front Microbiol* **4**, 26, doi:10.3389/fmicb.2013.00026 (2013).
53 Catlett, N. L., Lee, B.-N., Yoder, O. C. & Turgeon, B. G. Split-marker recombination for efficient targeted deletion of fungal genes. *Fungal Genet News* **50**, 9-11 (2002).
54 Punt, P. J., Oliver, R. P., Dingemanse, M. A., Pouwels, P. H. & van den Hondel, C. A. Transformation of *Aspergillus* based on the hygromycin B resistance marker from *Escherichia coli*. *Gene* **56**, 117-124, doi:10.1016/0378-1119(87)90164-8 (1987).
55 Al Abdallah, Q., Ge, W. & Fortwendel, J. R. A simple and universal system for gene manipulation in *Aspergillus fumigatus*: in vitro-assembled Cas9-guide RNA ribonucleoproteins coupled with microhomology repair templates. *mSphere* **2**, doi:10.1128/mSphere.00446-17 (2017).
56 Nodvig, C. S., Nielsen, J. B., Kogle, M. E. & Mortensen, U. H. A CRISPR-Cas9 System for Genetic Engineering of Filamentous Fungi. *PLoS One* **10**, e0133085, doi:10.1371/journal.pone.0133085 (2015).

57 Macheleidt, J. *et al*. Transcriptome analysis of cyclic AMP-dependent protein kinase A-regulated genes reveals the production of the novel natural compound fumipyrrole by *Aspergillus fumigatus*. *Mol Microbiol* **96**, 148-162, doi:10.1111/mmi.12926 (2015).
58 Gravelat, F. N. *et al*. *Aspergillus* galactosaminogalactan mediates adherence to host constituents and conceals hyphal beta-glucan from the immune system. *PLoS Pathog* **9**, e1003575, doi:10.1371/journal.ppat.1003575 (2013).
59 Paul, S. *et al*. AtrR Is an essential determinant of azole resistance in *Aspergillus fumigatus*. *mBio* **10**, doi:10.1128/mBio.02563-18 (2019).
60 Paul, S., Klutts, J. S. & Moye-Rowley, W. S. Analysis of promoter function in *Aspergillus fumigatus*. *Eukaryot Cell* **11**, 1167-1177, doi:10.1128/EC.00174-12 (2012).
61 Jhingran, A. *et al*. Tracing conidial fate and measuring host cell antifungal activity using a reporter of microbial viability in the lung. *Cell Rep* **2**, 1762-1773, doi:10.1016/j.celrep.2012.10.026 (2012).
62 Sheppard, D. C. *et al*. Novel inhalational murine model of invasive pulmonary aspergillosis. *Antimicrob Agents Chemother* **48**, 1908-1911, doi:10.1128/AAC.48.5.1908-1911.2004 (2004).
63 Liu, H., Lin, J., Phan, Q. T., Bruno, V. M. & Filler, S. G. Epidermal growth factor receptor signaling governs the host inflammatory response to invasive aspergillosis. **15**, e02671-02624, doi:doi:10.1128/mbio.02671-24 (2024).
64 Paul, S., Stamnes, M. A. & Moye-Rowley, W. S. Chromatin immunoprecipitation in *Aspergillus fumigatus*. *Methods Mol Biol* **3028**, 153-163, doi:10.1007/978-1-0716-5222-0_11 (2026).
65 Thorn, H. *et al*. Biotinylation-dependent near-neighbor analysis for identification of septation regulators in *Aspergillus fumigatus*. *bioRxiv*, doi:10.64898/2026.09.17.752449 (2026).

Table 1. Functional classes over-represented among the genes whose expression depends on WrpA in vitro, with their expression in the infected lung.

Gene set	Functional class	Genes in set / in class	Fold enrichment	FDR	Median RPKM in vivo	% expressed in vivo
Reduced in the Δ*wrpA* mutant	Translation and ribosome	68 / 175	9.8	1×10^{-49}	674.7	99%
	Secondary metabolite biosynthesis	12 / 55	5.5	5×10^{-6}	0.0	17%
Increased in the Δ*wrpA* mutant	Transporters and permeases	149 / 547	1.9	3×10^{-15}	2.1	40%
	Oxidoreductases	157 / 793	1.4	3×10^{-5}	4.1	47%
	Cell wall and glycan-active enzymes	54 / 247	1.5	2×10^{-3}	0.1	33%
	Secondary metabolite biosynthesis	17 / 55	2.2	2×10^{-3}	0.7	41%
	Carbohydrate metabolism	25 / 99	1.8	4×10^{-3}	1.0	40%

A gene was counted as reduced or increased in the Δ*wrpA* mutant if its transcript level differed from that of Af293 by at least two-fold with an adjusted *P* value below 0.05, determined with DESeq2 over a universe of 10,130 genes, during growth in Aspergillus minimal medium (AMM) at pH 6.5 with low zinc and low iron. Functional classes were assigned from the UniProt annotation of the Af293 proteome and tested by one-sided hypergeometric test with Benjamini-Hochberg correction; every class reaching an FDR below 0.05 is shown. Fold enrichment is the proportion of the gene set belonging to the class divided by the proportion of all annotated genes belonging to it, and "Genes in set / in class" gives the number of set members in the class and the total number of annotated genes in that class. Expression in vivo is the mean RPKM in corticosteroid-immunosuppressed mice at day 4 of infection, the time point at which lung fungal burden was measured, and a gene is counted as expressed at 5 RPKM or above. For reference, the median across all genes was 20.4 RPKM and 71% were expressed by this criterion.

Table 2. Transcription factors that are targets of WrpA.

Gene Symbol	Gene Name	Description	Log2-fold change (Δ*wrpA*/Af293)		WrpA Binding Score	In vivo expression (RPKM)[c]
			AMM[a]	DMEM[b]		
AFUA_1g01100		Fungal specific transcription factor	3.20[d]	0.65[d]	303	51
AFUA_2g09890	*ndt80*	Ndt80/PhoG transcription factor	2.58[d]	3.58[d]	58	9
AFUA_3g05760	*fcr1*	C6 transcription factor	0.52[d]	-1.19[d]	885	244
AFUA_4g10160	*amyR*	Zn(II)2Cys6-type transcription factor	0.67[d]	-1.26	479	18
AFUA_6g07010	*rosA*	Zn(II)2Cys6-type transcription factor	2.44[d]	3.42[d]	142	9
AFUA_7g00130	*nscR*	C6 transcription factor	5.97[d]	2.63[d]	70	119

[a]Aspergillus minimal medium with low Zn and Fe, 37°C for 24 h

[b]Dulbecco's modified Eagle medium 37°C for 6 h

[c]In lungs of cortisone acetate immunosuppressed mice after 4 d of infection

[d]Adjusted $p < 0.05$

Table 3. Functional classes over-represented among common genes altered in the Δ*wrpA, gpdA-ndt80*, and *gpdA-nscR* strains.

Gene set	Functional class	Genes in set / in class	Fold enrichment	FDR	Median RPKM in vivo	% expressed in vivo
Reduced in all three strains	C2H2 zinc-finger proteins	2 / 29	18.7	0.015	44.5	50%
Increased in all three strains	Short-chain dehydrogenases and reductases	5 / 79	8.1	6×10^{-3}	0.0	20%
	Glycoside hydrolase family 3, C-terminal domain	2 / 15	17.1	0.02	0.7	0%
	Transporters and permeases	10 / 547	2.3	0.021	0.0	10%
	Glycoside hydrolase family 3	2 / 17	15.1	0.021	0.7	0%
	Secondary metabolite biosynthesis	3 / 55	7.0	0.022	700.9	67%
	Fungal cellulose-binding domain	2 / 14	18.3	0.022	0.0	0%
	Fungal-specific transcription factor domain	2 / 14	18.3	0.029	0.7	0%
	Sugar transporters of the major facilitator superfamily	4 / 85	6.0	0.037	0.0	0%

A gene was counted as reduced or increased in a strain if its transcript level differed from that of Af293 by at least two-fold with an adjusted P value below 0.05.

Table 4. Functional classes over-represented in the two arms of the WrpA regulon defined by transcription factor occupancy.

Gene set	Functional class	Genes in set / in class	Fold enrichment	FDR	Median RPKM in vivo	% expressed in vivo
Circuit core (bound by all three factors)	Transcription factors	39 / 408	2.6	2×10^{-7}	60.3	97%
	Cell wall and glycan-active enzymes	21 / 247	2.3	1×10^{-3}	61.5	86%
	Iron acquisition and siderophores	7 / 44	4.4	3×10^{-3}	206.4	71%
	Carbohydrate metabolism	10 / 99	2.8	6×10^{-3}	78.1	70%
	Lipid and fatty acid metabolism	13 / 162	2.2	1×10^{-2}	115.9	100%
WrpA-only (bound by WrpA alone)	Transcription factors	51 / 408	1.6	4×10^{-3}	20.8	88%
	Transporters and permeases	66 / 547	1.5	4×10^{-3}	19.0	74%
	Iron acquisition and siderophores	9 / 44	2.5	0.022	49.8	67%

A gene was scored as bound when a peak for that factor overlapped the window from 1,500 bp upstream to 500 bp downstream of the gene start, strand-aware, with peaks lying in the gene body beyond +500 bp excluded. The circuit core is the 364 genes bound by WrpA, Ndt80 and NscR; the WrpA-only set is the 807 genes bound by WrpA alone.

Supplementary Files

This is a list of supplementary files associated with this preprint. Click to download.

- WrpAsupplementaryfigures20261102.pdf
- TableS8prmers.xlsx
- TableS5gpdAnscRvsAf293.xlsx
- TableS3wrpAChIPseq.xlsx
- TableS2wrpAvsAf293DMEM.xlsx
- TableS1wrpAvsAf293AMM.xlsx
- TableS7NscRChIPseq.xlsx
- TableS6Ndt80ChIPseq.xlsx
- TableS4gpdAndt80vsAf293.xlsx